iScience

CellPress
OPEN ACCESS

Review

Recent advances in the fabrication of 2D metal oxides

Huaguang Xie,[1] Zhong Li,[1,*] Liang Cheng,[1] Azhar Ali Haidry,[2] Jiaqi Tao,[2] Yi Xu,[3] Kai Xu,[4] and Jian Zhen Ou[1,4,*]

SUMMARY

Atomically thin two-dimensional (2D) metal oxides exhibit unique optical, electrical, magnetic, and chemical properties, rendering them a bright application prospect in high-performance smart devices. Given the large variety of both layered and non-layered 2D metal oxides, the controllable synthesis is the critical prerequisite for enabling the exploration of their great potentials. In this review, recent progress in the synthesis of 2D metal oxides is summarized and categorized. Particularly, a brief overview of categories and crystal structures of 2D metal oxides is firstly introduced, followed by a critical discussion of various synthesis methods regarding the growth mechanisms, advantages, and limitations. Finally, the existing challenges are presented to provide possible future research directions regarding the synthesis of 2D metal oxides. This work can provide useful guidance on developing innovative approaches for producing both 2D layered and non-layered nanostructures and assist with the acceleration of the research of 2D metal oxides.

INTRODUCTION

In 2004, Novoselov et al. used scotch tape to successfully exfoliate graphene from graphite (Novoselov et al., 2004). Since then, two-dimensional (2D) materials have been developed rapidly owing to their interesting traits of atomically thin crystals, which brought in unique optoelectronic properties, ultrahigh surface volume ratio, excellent mechanical properties, and rich surface chemical activity as compared to their bulk counterparts (Zhang, 2015). So far, various 2D nanomaterials have been widely reported, from the original graphene to the later transition metal dichalcogenides (TMDs including WS_2, MoS_2, WSe_2, $MoSe_2$, ReS_2, TaS_2, etc.) (Lv et al., 2015; Manzeli et al., 2017; Saeed et al., 2020), noble metal dichalcogenides (NMDs: PtS_2, PtSe, PdSe, etc.) (Pi et al., 2019), elemental 2D materials (e.g. black phosphorus (BP), silicone, tellurium, etc.) (Lin et al., 2020; Mannix et al., 2018; Si et al., 2021), layered double hydroxides (LDHs) (Lv et al., 2019), Mxenes (Anasori et al., 2017), graphitic carbon nitride (g-C_3N_4) (Wang et al., 2021b), metal-organic frameworks (MOFs) (Chen et al., 2021b), covalent-organic frameworks (COFs) (Chen et al., 2021a) and metal oxides (MOXs) (Mahmood et al., 2019), etc. In particular, 2D MOXs present excellent performance in electronics, optoelectronics, electrochemistry, sensors, energy storage, catalysis, and other fields, thus gaining extensive research and concern globally.

Generally, 2D MOXs can be divided into two categories according to their crystal structure: layered and non-layered. There are several layered MOXs materials assembled from M-O (M: V, Mo, or Mn) octahedral (Apte et al., 2020; Haque et al., 2018; Nagyné-Kovács et al., 2020; Ren et al., 2020; Rui et al., 2013; Zhang et al., 2018), in which the in-plane atoms are connected via strong chemical bonding, and the stacking layers are combined via weak van der Waals (vdW) interaction. Recently, a layered crystal structure with the unique planar hexagonal coordination is found across various oxides of Ti, Mn, Fe, Co, Ni, Cu, Al, Gd, and Ge, which is distinctly different from their conventional non-polarized crystal structures seen at room temperature (Zhang et al., 2021a). Such a crystal structure is similar to those of layered hexagonal transition metal chalcogenides (TMCs), greatly enriching the 2D layered family of metal oxides. On the other hand, the crystal structures of most MOXs in the ultrathin 2D morphology are not layered as all the atoms are connected by the strong chemical bonding, resulting in abundant unsaturated dangling bonds on the surface or along the edges, thus inducing a high activity and high-energy surfaces, such as In_2O_3 (Cho and Huh, 2010), TiO_2 (Tao et al., 2011), SnO_2 (Lv et al., 2021), ZnO (Mahmood et al., 2021), and WO_3 (Yao et al., 2019). In addition, it is worth mentioning that lamellar metal oxides with foreign

[1]Key Laboratory of Advanced Technologies of Materials, Ministry of Education, School of Materials Science and Engineering, Southwest Jiaotong University, Chengdu 610031, China

[2]College of Materials Science and Technology, Nanjing University of Aeronautics and Astronautics, Nanjing 211106, China

[3]School of Materials Science and Engineering, Nanchang University, Nanchang 330031, China

[4]School of Engineering, RMIT University, Melbourne 3000, Australia

*Correspondence: nuaalizhong@163.com (Z.L.), jianzhen.ou@rmit.edu.au, jzou@swjtu.edu.cn (J.Z.O.)

https://doi.org/10.1016/j.isci.2021.103598

ions being accommodated in the gaps between atomic layers also attracted extensive research (Ding et al., 2017; Kalantar-Zadeh et al., 2016), of which perovskite (Ma et al., 2018) is the typical example.

Although the group of 2D metal oxide nanomaterials has abundant members and many of them have been successfully prepared, it is still a critical challenge to develop a scalable, simple, effective, and economical approach for their synthesis. Therefore, in recent years, great progress has been made in the preparation of 2D MOXs, which can be roughly divided into top-down exfoliation, bottom-up synthesis, and liquid metal strategy. The top-down exfoliation is achieved by layering the main crystal precursors of MOXs (generally layered oxides) into the element layers. The bottom-up synthesis is to obtain the atoms/molecules of the required metal and oxygen and limit their growth in the 2D direction under specific conditions. The liquid metal strategy is to synthesize the ultrathin 2D MOXs upon the surface of liquid metals or alloys through the self-limiting reaction.

In general, owing to their intriguing properties, 2D MOXs are attracting rapid interest and great progress has been made in synthetic strategies. Although several articles have already described parts of synthesis methods for 2D MOXs (Dou et al., 2017; Mei et al., 2017; Zavabeti et al., 2020; Zhou et al., 2019; Zhuang et al., 2020), there have been a number of emerging highlights including hexagonal layered MOXs, 2D large-area non-layered MOXs, ultrathin amorphous MOXs, and 2D rare-earth oxides (REO). Their associate synthesis methods, such as metal-gas interfacial limited reaction, orientation-driven crystalline cleavage, gas-assisted exfoliation, and liquid metal-derived fabrication, also demonstrate significant advancement in achieving the 2D ultrathin morphology. Therefore, in this review, we focused on the aforementioned highlights along with the recent achievements of producing 2D MOXs using conventional top-down and bottom-up approaches to provide a timely summary and critical discussion of the state-of-the-art synthetic strategies of the fast-moving field of 2D MOXs. To commence with, we outline the categories and crystal structures of 2D MOXs and then summarize the emerging synthetic strategies as well as the new improvements of traditional methods. Finally, challenges, perspectives, and future research focus of 2D MOXs are also provided.

BASICS OF 2D METAL OXIDES

According to the distinction of structural characteristics, 2D MOXs can be divided into three categories, which are layered, lamellar, and non-layered MOXs. The layered MOXs include the traditional layered MOXs, emerging hexagonal MOXs, and LDHs. MoO_3 and V_2O_5 are representative of traditional layered MOXs. As the crystal structures shown in Figure 1A and 1B, MoO_3 possesses a layered structure in which each layer is predominantly composed of distorted MoO_6 octahedral in an orthorhombic crystal (Yang et al., 2017a) and 2D V_2O_5 generally has an orthorhombic crystal structure, consisting of zigzag double chains of square-based VO_5 pyramids, bonded together with corner-shared bridge oxygen atoms (Rui et al., 2013). Zhang et al. first reported the exfoliated method to obtain layered planar hexagonal metal oxide, including mono- and few-layered hexagonal TiO_2 (Figure 1C), Fe_2O_3, Ni_2O_3, etc., derived from the metal-gas interface (Zhang et al., 2021a). Similar to those of layered hexagonal TMCs (Wang et al., 2021e), each atomic layer is composed of a hexagonal ring that accommodates both the metal and oxygen atoms. In the vertical view, a layer of metal atoms is sandwiched by two layers of oxygen atoms, forming a typical "sandwich" structure. Figure 1D shows the typical crystal structure of LDHs, with metal cations occupying the center of the octahedron and the vertices containing hydroxide shared ions to form 2D layers (Ou et al., 2021). Moreover, charge-balancing anion or solvation molecules (CO_3^{2-}, Cl^-, and SO_4^{2-}) are located in the gap of the hydrated interlayer. In contrast, in the lamellar MOXs, atoms or ions are bonded to the oxide layer by weak electrostatic forces. For instance, Bi_2O_2Se (Chen et al., 2018) consists of planar covalently bonded oxide layers (Bi_2O_2) sandwiched by Se square arrays with relatively weak electrostatic interactions as shown in Figure 1E (Luo et al., 2021). As another example of inorganic perovskites, $CaTiO_3$ possesses a similar structure (Li et al., 2013).

Non-layer structured MOXs are reformed via chemical bonding in three dimensions. Examples of non-layer structured MOXs are CeO_2, SnO_2, WO_3, and In_2O_3, which do not have a general formula and their crystal structures could be different from one another. As shown in Figure 1F, CeO_2 is one typical example of non-layered structured MOXs whose structure is formed by a face-centered cubic unit cell of cations and the anions occupying the space of the octahedral (Song et al., 2017).

Ultrathin 2D MOXs can be electrically insulating, conductive, or semiconducting, depending on their band structure and doping level, making them the ideal materials for designing new types of electronic devices.

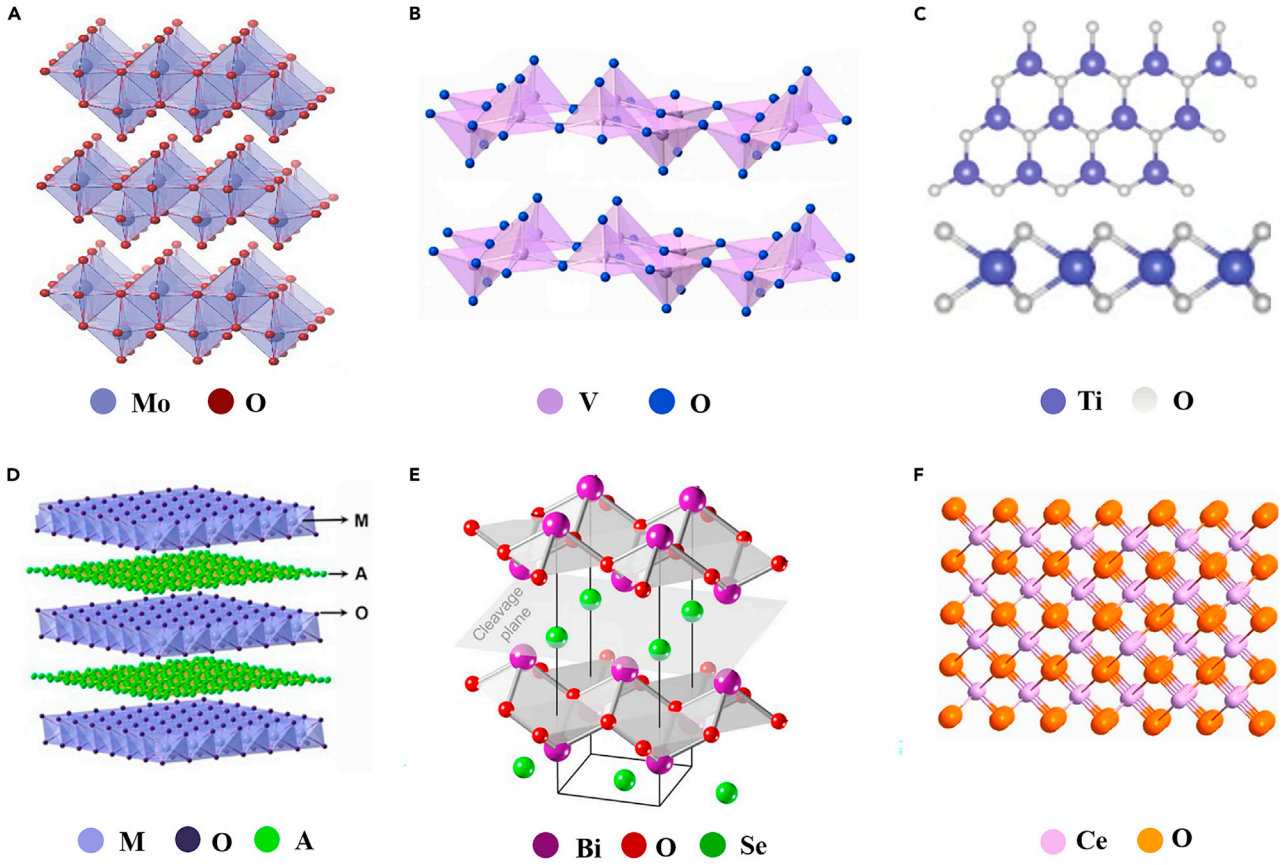

Figure 1. Crystal structure diagram of various 2D MOXs

(A) MoO_3 (Yang et al., 2017a) Copyright 2017, Wiley-Blackwell.

(B) V_2O_5 (Tan et al., 2017) Copyright 2017, American Chemical Society.

(C) h-TiO_2 (Zhang et al., 2021a) Copyright 2021, Springer Nature.

(D) LDHs. M, metal cations; O, hydroxide ions; A, charge-balancing anion or solvation molecule (Tan et al., 2017) Copyright 2017, American Chemical Society.

(E) Bi_2O_2Se (Chen et al., 2018) Copyright 2018, American Association for the Advancement of Science.

(F) CeO_2 (Tan et al., 2017) Copyright 2017, American Chemical Society.

The fine thickness at the atomic scale gives 2D MOXs interesting properties, such as optical transparency and mechanical flexibility, which can also be used in flexible electronics and new optoelectronic devices. Other attractive features include high theoretical capacitance, large surface area, and the potential for oxidation-reduction reactions, making 2D MOXs ideal for high energy density supercapacitors and batteries. In addition, their excellent photoelectric properties and high surface chemical reactivity make them suitable for use as photocatalysts as well as gas and biosensors (Dral and ten Elshof, 2018; Fine et al., 2010; Haque et al., 2018; Khan et al., 2021; Kumbhakar et al., 2021; Li et al., 2021c; Shangguan et al., 2021).

It is worth noticing that amorphous 2D MOXs as a class of disordered structures with many dangling bonds, activity sites, and ion channels have also attracted extensive attention in recent years due to their superior performance in energy storage, catalysis (Jia et al., 2020). As compared to their crystalline counterparts, amorphous 2D MOXs are isotropic with no grain boundaries, and thus possess more dangling bonds and reactive sites exhibiting more special physical and chemical properties (Haque et al., 2019; Yan et al., 2021). For example, amorphous 2D NiO and SnO_x usually present higher photocatalytic performance than those with crystalline structures (Yuan et al., 2020). In addition, the basis of obtaining high-quality 2D MOXs by various preparation methods, heterogeneous structure design, doping, introducing defects, and other strategies can greatly optimize the intrinsic character of these materials and expand their application scope. Examples include the generation of enhanced surface plasmon resonance across the entire visible light and part of the near-infrared region in 2D MoO_x enabled by ions and/or oxygen vacancies. Among

them, the localized manipulation of d-electron states is the major factor for transition MOXs to achieve abundant high free electron concentration and mobility to generate plasmon resonances in the visible and near-infrared regions (Alsaif et al., 2021). In addition, similar plasmonic properties have appeared in 2D amorphous MoO_3 quantum dots and are expected to be used for Raman spectroscopy detection (Alsaif et al., 2016; Ge et al., 2021; Guo et al., 2019; Li et al., 2018; Liu and Xu, 2018; Ren et al., 2019; Yin et al., 2021; Shangguan et al., 2021). Further, it has been proved that 2D heterostructures, constructed from vdW stacking (2D vertical heterostructures) or edge covalent bonding (2D lateral heterostructures) of different 2D materials, can not only address the problem of insufficient performance of a single 2D material in applications such as photodetectors and gas sensing but also generate many peculiar properties through the synergistic advantages of individual 2D materials. For example, the large area heterostructures of atomically thin p-SnO/n-In_2O_3 exhibit both outstanding photodetectivity and photoresponsivity under the illumination of the 280 nm light. This excellent performance is due to the narrow bandgap of the staggered band at the p-n junction formed by the high-quality SnO/In_2O_3 heterostructure (Alsaif et al., 2019a). Low-dimensional magnetic materials (including 2D oxides, etc.) possess excellent magnetic properties which originate from the defects such as vacancy, doping, adatom, and dangling bonds, which can be important in advancing electronics, data storage, and even biomedical fields. For example, MoO_3 can be induced magnetic ordering through hydrogenation or external strain; besides, monolayer MnO_2 is reported to be inherently ferromagnetic, which is a potential candidate for the next-generation devices with faster processing and large data storage capacity (Sethulakshmi et al., 2019). Compared with other 2D materials (such as telluride (Siddique et al., 2021)), 2D MOXs take on stable, adjustable, excellent physical and chemical properties, and enjoy an enviable position in future various applications. Therefore, the preparation of 2D MOXs has become a more important section in scientific research and practical applications.

FABRICATION METHODS OF 2D METAL OXIDES

With fascinating properties and numerous potential applications, 2D MOXs have gained growing attention, which promotes synthetic methods to be developed rapidly. Up to now, these methods can be divided into three main following strategies including top-down, bottom-up, and the liquid metals-assisted approach (Sun et al., 2017). Usually, the top-down approach is applicable for 2D layered MOXs, while bottom-up synthesis is not limited to the oxide crystal structures (Kalantar-Zadeh et al., 2016). The former covers 3D layered crystals into large numbers of mono- and few-layered 2D MOXs through an energy input such as mechanical force, sonication, ion intercalation or exchange, and electrochemical methods. Meanwhile, in the latter, the atoms or molecules are grown or assembled along the lateral direction on the suitable substrate or template in a specific environment, finally forming ultrathin 2D MOXs. As for the emerging liquid metal strategy, the oxide layer formed on the surface of liquid metal or alloy is often exfoliated through printing and other processes.

Top-down exfoliation

After successfully exfoliating graphene from graphite through the adhesive tape, many types of 2D metal oxide nanosheets have been prepared through the top-down approach. This method is not only relatively simple and scalable but also capable of maintaining high crystallinity. However, the thickness and lateral size of nanosheets obtained by this method are uncontrollable. Moreover, there is an obvious restriction for the layered host crystal, which greatly limits its application range. The top-down approaches mainly include mechanical force-assisted exfoliation, soft chemical exfoliation, and electrochemical exfoliation.

Mechanical force-assisted method

Because researchers obtained graphene by mechanical exfoliation, mechanical exfoliation has become demanding to obtain 2D materials. However, there are only a few reports on obtaining mono- and few-layered planar MOXs by mechanical exfoliation in recent progress. Zhang et al. achieved uniform growth of layered hexagonal metal oxide at the metal-gas interface within a specific condition, in which bulk metal surface was polished into the nanoscale roughness to minimize the roughness and the defect-driven promotion of oxidation, and an oxygen-deficient environment was applied to slow down the oxygen penetration into metal lattices (Zhang et al., 2021a). Upon the formation of the layered oxide structure, single and few atomic layers were mechanically exfoliated by stamping the polished metal face onto the desired substrate. Such an exfoliation is highly reproducible and the lateral size of 2D oxide sheets is strongly dependent on the metal surface roughness. The complete synthesis process is shown in Figure 2A. At

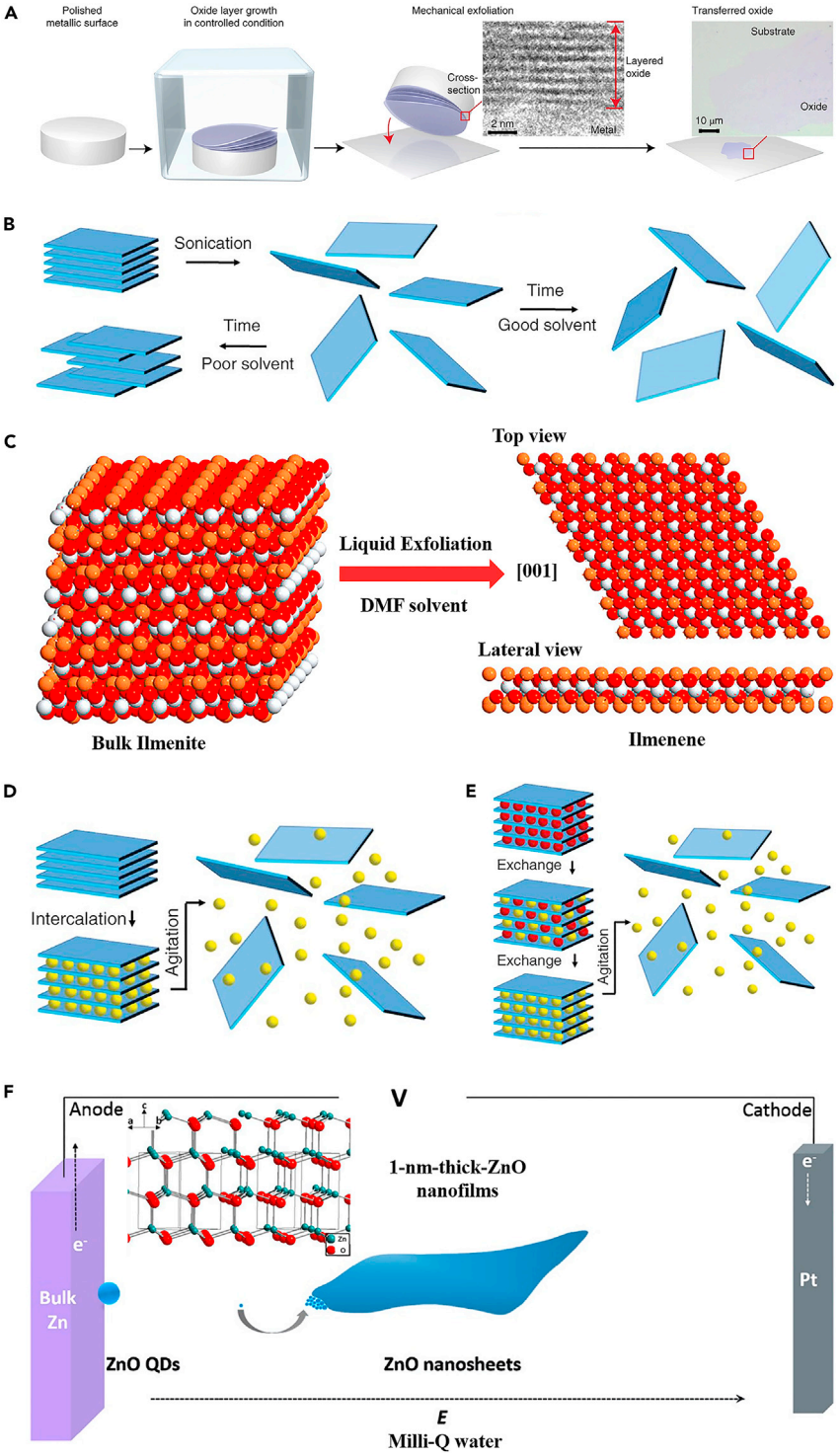

Figure 2. The schematic diagram of various top-down exfoliation methods

(A) The schematic diagram of layered growth and subsequent mechanical exfoliation (Zhang et al., 2021a) Copyright 2021, Springer Nature.

(B) The schematic diagram of ultrasonic-assisted liquid-phase exfoliation (Xiong et al., 2020) Copyright 2020, World Scientific Publishing Co. Pte Ltd.

(C) The schematic of the liquid-phase exfoliation of bulk ilmenite in DMF to ilmenene (Puthirath Balan et al., 2018a) Copyright 2018 American Chemical Society.

Figure 2. *Continued*
(D) The schematic diagram of ion intercalation-assisted exfoliation (Xiong et al., 2020) Copyright 2020, World Scientific Publishing Co. Pte Ltd.
(E) The schematic diagram of ion exchange-assisted exfoliation (Xiong et al., 2020) Copyright 2020, World Scientific Publishing Co. Pte Ltd.
(F) Apparatus for reagent-free electrophoretic synthesis for the formation of metal oxide nanosheets (Hou et al., 2017) Copyright 2017, American Chemical Society.

present, nine types of 2D hexagonal metal oxide monolayers (TiO_2, MnO, Fe_2O_3, CoO, Ni_2O_3, Cu_2O, Al_2O_3, GeO_2, and Gd_2O_3) have been successfully prepared.

As compared to the traditional mechanical exfoliation method, Huang et al. reported an improved exfoliation method that introduced two steps (oxygen plasma cleaning and heat treatment) to enhance and homogenize the adhesion between the outermost sheet and the contacted substrate (Huang et al., 2015). The environmental adsorbents can be effectively removed from the substrate by oxygen plasma cleaning before the exfoliation stage. Further additional heat treatment can maximize the uniform contact area at the interface between the source crystal and the substrate. These simple process steps have increased the yield and the area of the transferred flakes by more than 50 times compared to the established exfoliation. Furthermore, Bayazit et al. reported an interesting microwave-modulated solid-state approach that not only rapidly exfoliated graphite but also self-healed the defects on the graphene (Bayazit et al., 2021). This fast and green microwave exfoliation process is predicted to yield monolayered high-quality 2D materials. Although there have been no reports of 2D MOXs prepared by the above methods, they are still an important complement to the exfoliating method of MOXs.

In addition to the atmospheric environment, MOXs can also be exfoliated in a liquid environment. Liquid-phase exfoliation usually involves sonicating the layered crystals in certain stabilizing liquids. Ultrasonic waves are usually used to break the vdW forces between the layers, while the applied forces do not affect the strong in-plane covalent bond interactions in layers (Figure 2B). Ultrasonic-assisted liquid-phase exfoliation has led to the synthesis of layered 2D MOXs, such as MoO_3 (Hanlon et al., 2014) and V_2O_5 (Tan et al., 2017). The fundamental principle is based on the mechanical energy of an ultrasonic wave which generates a large number of cavitation bubbles around the bulk material. The micro-jet and vibration waves generated at the bubble burst increase the interlayer distance under the non-uniform pressure to promote the interlayer separation of layered materials and finally obtain the dispersion liquid containing 2D nanosheets (Huo et al., 2015). Here, the selection of solvent is a key factor affecting the stability of the exfoliated nanosheets (Alsaif et al., 2016). Specifically, the stabilized liquids can be certain solvents, surfactants, or polymer solutions. For surfactants or polymers, the repulsive forces between the adjacent surfactants (or polymers) and the nanosheets remain stable. In addition, the vdW interaction strengths between the solvents with appropriate surface-energy or solubility parameters and the 2D nanosheets are similar to those of binding strength between nanosheets, thus preventing the aggregation of nanosheets (Hanlon et al., 2014). More importantly, the relatively high compatibility of surface energy between layered materials and solvents can effectively reduce the corresponding exfoliation energy, thus improving the exfoliation efficiency (Fujihara et al., 2004). Taking the Hansen solubility parameters into account, Coleman et al. found that *N*-methy1-2-pyrrolidone (NMP), *N*, *N*-dimethylformamide (DMF), and *N*-cyclohexy1-2-pyrrolidone are the best solvents (Hanlon et al., 2014). However, the high boiling point (>150°C) of these dispersions restricts their usage in flexible devices along with the toxic nature of the exfoliation solvents. Finding suitable solvents, especially with the features of low boiling point, non-toxic, and pollution-free, has become an important direction of developing economical and green preparation methods. Kim et al. reported a direct exfoliation of 2D materials in deionized water via temperature control, without using any chemicals or surfactants (Kim et al., 2015). The results show that 2D materials with good dispersion stabilities in water can be synthesized by ultrasonic treatment at high temperatures. This use of deionized water not only enables cost-effective industrial and commercial applications but also facilitates research that is required for water-based experiments. Recently, combined with the characteristics of the self-limiting reaction of liquid gallium metal, the liquid gallium was ultrasonic treated in deionized water and then through a centrifugation and annealing process to obtain the ultrathin 2D Ga_2O_3 nanosheets (Syed et al., 2017).

2D non-layered nanosheets have been considered inaccessible to obtain by exfoliation due to the absence of anisotropy in the 3D bonding network. However, many non-layered materials have perfect cleavage planes, which are generally the closely arranged planes of atoms with the largest surface spacing and

the least interconnection force (Xu et al., 2021). Therefore, owing to the anisotropic in-plane and out-of-plane cleavage bonding, non-layered materials with perfect cleavage planes are easy to fracture along the direction of cleavage, thus forming a smooth surface of atoms under certain conditions. Furthermore, when the external energy exceeds the cleavage energy, the non-layered material with the cleavage plane can be exfoliated into 2D nanosheets along its cleavage direction. The exfoliation of these natural minerals has opened a new possibility for obtaining 2D non-layered natural oxides. For example, Puthirath et al. obtained a new 2D non-layered material named "hematene", which was exfoliated via employing ultrasonic-assisted liquid-phase exfoliation of natural iron ore hematite (α-Fe_2O_3) in a DMF solvent along the two different crystallographic planes (Puthirath Balan et al., 2018b). Similarly, previous reports have also demonstrated that "chromiteen" (Yadav et al., 2018) and "ilmenene" (Puthirath Balan et al., 2018a) can also be obtained from chromite ore and titanate ore ilmenite ($FeTiO_3$) (Figure 2C), respectively. Additionally, Liu et al. found that the orientation of the nanosheets was consistent with the cleavage orientation of the original material, hence for the first time successfully exfoliating a class of non-layered MOXs (Liu et al., 2019). The non-layered α-hydroxyl iron oxide shows weaker atomic bonds along the (010) and (100) cleavage planes. When sufficiently large ultrasonic energy was applied, the resulting shear force can generate 2D nanosheets by cleaving crystalline materials along with the α-hydroxyl iron oxide along (010) and (100) orientations. Such an emerging strategy for the exfoliation of non-layered metal oxide materials provides a new train of thought, which successfully exfoliated TiO_2, Al_2O_3. However, it should be noted that some MOXs (Cr_2O_3, Sb_2O_4, etc.) cannot be processed without cleavage plane into 2D morphology in this way. In summary, this method provides valuable insights and guidance for developing a simple, universal, and pollution-free method to produce 2D materials. In addition, this method has become highly in demand because the traditional exfoliation methods cannot provide such efficiency.

Compared with ultrasonic-assisted liquid-phase exfoliation, 2D amorphous materials can be obtained by supercritical carbon dioxide (SC-CO_2)-assisted exfoliation (Liu et al., 2017, 2020; Ren and Xu, 2018). Liu et al. successfully obtained amorphous 2D MoO_3 nanosheets, in which it combined the oxidation of MoS_2 and subsequent SC-CO_2 treatment. Firstly, by annealing single or several layers of MoS_2 with a complete lattice structure, oxygen atoms can replace sulfur atoms to realize the incorporation of oxygen in MoS_2. Given that the adsorption strength of small molecules on an amorphous surface is stronger than that on a crystal surface, the adsorption of CO_2 can lead to the stabilization of amorphous MoO_3, thus realizing the transformation to the amorphous structure (Liu et al., 2017). Although SC-CO_2 shows promising prospects in the fabrication of 2D amorphous materials, the related mechanism induced by SC-CO_2 is still unclear. Recently, Xu et al. revealed the amorphization mechanism by exploring the amorphization kinetics of MoO_{3-x} nanosheets induced by SC-CO_2 under different pressures. At lower pressure, the activation energy of amorphization is only about 0.5 eV, which mainly involves the fracture of the Mo-O bond and the formation of oxygen vacancy. At higher pressure, the activation energy required for amorphization is three times higher than at low pressure, mainly ascribed to the local shear-induced atomic rearrangement. It is worth noting that the two processes are not independent of each other (i.e. the formation of oxygen vacancy is still accompanied at high pressure) (Ge et al., 2021b). In addition to layered MOXs, ultrathin non-layered MOXs can be also obtained by the SC-CO_2-assisted exfoliation. For example, monocline (M) VO_2 is a non-layered material that can transform into rutile (R) VO_2, in which both phases possess tunnel-like structures, thus providing a special structural environment for the intercalation and diffusion of CO_2molecules. Zhang et al. successfully fabricated the defect-rich 2D non-layered VO_2 (M) nanosheets by the SC-CO_2-assisted method (Zhang et al., 2021b). The diffusion of CO_2 in the M-phase channel generated shear strain along the α-axis and induced atom rearrangement to form defects. When the temperature of the supercritical environment was higher than the metal–insulator transition temperature, the M-phase transforms into R-phase, and then the diffusion of CO_2 in the swelling R-phase lattice structure produced a strong shear strain along the c-axis. This strain contributed to the formation of many atomic defects in the 3D V-O bonding network, and the unstable defective network then collapsed to 2D nanosheets. Additionally, 2D oxygen-doped amorphous carbon nitride materials were prepared with the assistance of SC-CO_2, showing excellent photocatalytic activity due to increased surface area and abundant activity (Du et al., 2021). The SC-CO_2-assisted method provides a reference for the preparation of 2D amorphous MOXs, especially non-layered materials, from a limited source of precursors.

In summary, several mechanical force-assisted exfoliation approaches have been developed but with the following disadvantages. Firstly, the production yield of 2D MOXs by mechanical exfoliation is low. Secondly, the 2D MOXs obtained by liquid-phase exfoliation have poor controllability of thickness and

lateral size. Lastly, all of them are limited to the fabrication of 2D layered MOXs and only a few non-layered MOXs can be prepared successfully.

Soft chemical method

Soft chemical exfoliation includes both ion intercalation-assisted exfoliation (Figure 2D) and ion exchange-assisted exfoliation (Figure 2E). Given the strong negatively charged nature in MOXs (particularly lamellar MOXs), the interaction between the atomic layers is enhanced; thus, ultrasonic waves cannot be effectively used for delamination. Therefore, appropriate chemical force is required to overcome the strong electrostatic effect. The principle of ion intercalation is based on the transfer of molecules or ions under certain conditions into layers, resulting in layered structured strain expansion and increased layer spacing. With the weakening of the interlayer interaction, the main material finally forms the exfoliated dispersion in the appropriate environment.

Many layered oxides are mixed-valence compounds containing exchangeable interlayer of cationic counterions, thus can be exfoliated by ion exchange-assisted exfoliation. For example, lamellar crystals of Ti oxide tend to be negatively charged (because of the presence of Ti^{3+} and Ti^{4+} ions), and thus contain counter-ions such as Cs^{+} between the layers to ensure charge neutrality. By ions exchange in solutions, protons are exchanged into large volumes of organic ions (tetrabutylammonium cations), resulting in an increasing layer space, thus completing the exfoliated process (Nicolosi et al., 2013). However, layered MOXs, such as MoO_3, occur naturally in the form of monovalent compounds. This compound cannot be exfoliated by the ion-exchange method (Hanlon et al., 2014). Sricharan et al. reported an exfoliation of MoO_3 in a low boiling point solvent, which was carried out in 2-butanone for the first time and achieved the highest yield (Sricharan et al., 2020). Additionally, the MoO_3 dispersions in 2-butanone exhibited ultrahigh stability and did not undergo any chemical transformation even upon light exposure. The high stability and yield can be attributed to the favorable matching of surface energy between MoO_3 nanosheets and 2-butanone solvent. This further authenticates the importance of solvent selection for liquid-phase exfoliation. Soft chemical exfoliation is often combined with ultrasonic or shear force to promote exfoliation process, which reduces the time considerably. However, the high cost is also a disadvantage at the same time.

Electrochemical method

In contrast to traditional exfoliation methods, electrochemical exfoliation uses an electric current as a special driving force to carry external molecules or ions into the bulk material, thereby expanding their interlayer spacing. This method is eco-friendly because the electrolyte is recyclable, hence eliminating the chemical waste. In addition, the exfoliation reaction time is usually ranged from minutes to a few hours with very considerable yield. Electrochemical exfoliation is carried out in a typical three-electrode electrochemical cell which consists of three electrodes including a working electrode (WE), a counter electrode (CE) and a reference electrode (RE), a liquid electrolyte, and an external power source. For a general principle of electrochemical exfoliation, the electrolyte supports sufficient ion migration and provides adequate surface tension to prevent the restacking of exfoliated flakes. Once a suitable voltage is applied between the WE and RE, the insertion of the ionic material into the interlayer and subsequent electrolysis of intercalants promotes the significant structural expansion of the electrode materials, thus resulting in the delamination of the bulk material into suspended thin layers (Yang et al., 2020b).

Electrochemical exfoliation was initially used for producing graphene, which has been then further extended to the preparation of 2D MOXs (Aghamohammadi et al., 2020). For example, Yang et al. reported one-pot electrochemical potential-cycles exfoliation to fabricate nonconductive 2D layered birnessite-type manganese oxide utilizing non-layered metal as a starting precursor (Yang et al., 2021). Mono- and few-layered birnessite sheets can be obtained through a repeated process of anodic dissolution-cathodic deposition-cathodic exfoliation. In this method, instead of the use of insulating lamellar bulk metal oxide solids, non-vdW manganese metal with a good electrical conductivity was used as the electrode to avoid the incomplete stripping of the starting material and the obstruction of electrode conductivity. By controlling the potential scan rate, 2D layered Na-birnessite, Li-birnessite, and K- birnessite with adjustable thickness and cation content were obtained.

Reagent-free electrophoretic synthesis of 2D MOXs is another good option that yields pure nanosheets of oxides without the use of any additional reagents. Hou et al. reported a green method for cost-effective

Table 1. The summary of the top-down method for the fabrication of 2D MOXs

Synthesis methods	Advantages	Limitations	Materials	Thickness (nm)	Applications	Ref.
Mechanical exfoliation	Simple High quality	Low yield	h-TiO_2	0.55	Electronic device	(Zhang et al., 2021a)
Ultrasonic-assisted liquid-phase exfoliation	Simple Economical Scalable	Poor controllability	Ga_2O_3	6	Photocatalyst	(Syed et al., 2017)
			MoO_3	3–4	Supercapacitor	(Hanlon et al., 2014)
			V_2O_5	2.1–3.8	Lithium storage	(Zhang et al., 2017)
Cleavage plane-oriented exfoliation	Simple Economical	Poor scalability	TiO_2	0.41	–	(Liu et al., 2019)
SC-CO_2-assisted exfoliation	Amorphous structure	High cost	VO_2	–	–	(Zhang et al., 2021b)
Soft chemical exfoliation	Simple Moderate	Low efficiency High cost	MoO_3	5	Supercapacitors	(Sricharan et al., 2020)
Electrochemical exfoliation	Eco-friendly Efficiency High yield	Poor scalability	MnO_2	0.73	Zinc-ion batteries	(Yang et al., 2021)
			ZnO	1	Gas sensor	(Hou et al., 2017)

and rapid preparation of atomic metal oxide nanosheets (Hou et al., 2017). The reagent-free synthesis principle combined the anodic oxidation with electric-field-induced assembly (Figure 2F), in which metal oxide grains/quantum dots (QDs) were generated from the anode by electrolysis of water. They were charged and endowed with built-in dipoles by the applied DC electric field. As the applied electric fields were perpendicular to the electrode plane, QDs were assembled and aligned into 2D atomic nanosheets around the cathode with a very high transverse size to thickness ratio. The morphological studies indicated that ZnO nanosheets possess large lateral dimensions of ~10 μm along with a typical thickness of only 1 nm which can be produced only in 1 h under ambient conditions.

In conclusion, electrochemical exfoliation has the advantages of being environmental-friendly, economical, and efficient. However, only a small number of 2D MOXs have been prepared by this method at present, and there are certain challenges in expanding to a wider range of MOXs. The advantages and limitations of various top-down exfoliation methods as well as the thickness and applications of the obtained 2D MOXs are summarized in Table 1.

Bottom-up synthesis

In addition to the top-down approaches, the bottom-up synthesis strategy has been also rapidly developed especially for the 2D non-layered MOXs. Owing to the intrinsic isotropic chemical bonding in 3D directions, non-layered crystals usually exhibit particular morphologies to reach the lowest energy of the system and maintain excellent stability. Therefore, when the thickness of the nanostructure becomes atomically thin, the unsaturated dangling bonds are exposed on the surface and further hinder the synthesis of 2D non-layered MOXs, which need to be compensated to satisfy the surface electrostatics via electron redistribution, surface reconstruction, or adsorption of charged species. In addition, unlike the well-matched among the layered MOXs and substrate lattice, the non-layered MOXs materials usually exhibit completely different crystal orientations with the substrates, which increase the difficulty of preparation. Undoubtedly, the preparation of 2D non-layered materials faces enormous difficulties and challenges (Wang et al., 2017b).

Recently, some effective methods have been proposed to realize the synthesis of 2D non-layered MOXs materials by restraining the growth of special crystallographic facets. In the beginning, some non-layered 2D structures (including TiO_2 [Lan et al., 2018], WO_3 [Wang and Liu, 2015], and MoO_2 [Xiao et al., 2016]) were acquired by the wet chemical synthesis and template-assisted methods, in which surfactant agents and hard/soft templates were used to ensure the anisotropic growth. However, the challenges of residual organic contaminations, low crystal quality, and small size hinder the wider applications. Therefore, it is necessary to solve the aforementioned issues by optimizing the traditional wet chemical process. In comparison, as another common bottom-up synthesis, the precursor vapor aggregates and grows into 2D

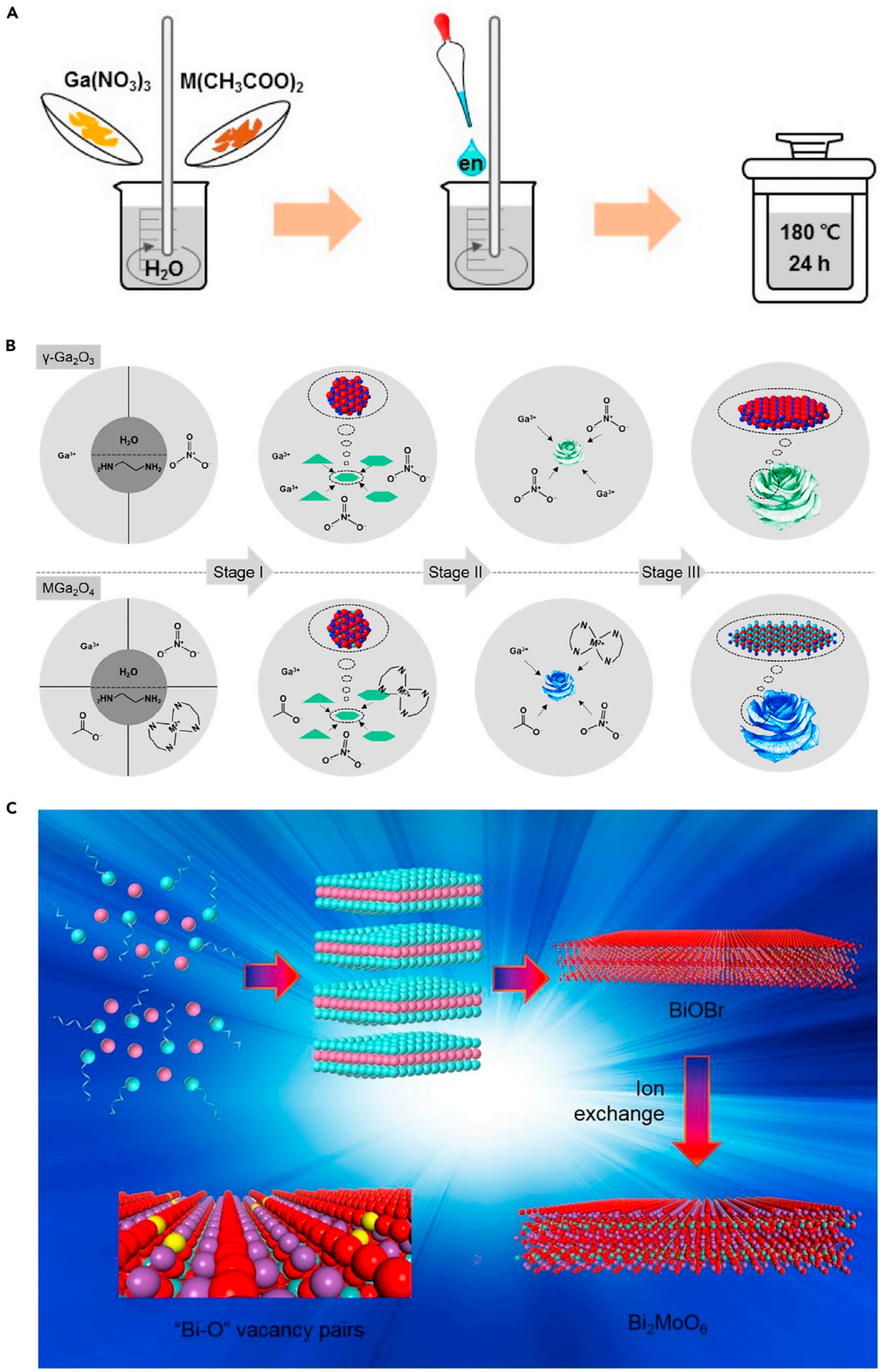

Figure 3. Bottom-up synthesis: hydrothermal/solvothermal synthesis of 2D MOXs

(A) The schematic diagram describing the formation process of spinel-type 2D oxide nanosheets (Yang et al., 2019)
Copyright 2019, American Chemical Society.

Figure 3. *Continued*
(B) Schematic diagrams describing the formation of γ-Ga_2O_3 nanosheets, MGa_2O_4 nanosheets, and their self-assembling into nanoflowers (Yang et al., 2019) Copyright 2019, American Chemical Society.
(C) Schematic template-assisted strategy to fabricate freestanding Bi_2MoO_6 ultrathin nanosheet (Di et al., 2019) Copyright 2019, Elsevier BV.

nanomaterials on an appropriate substrate during the chemical vapor deposition (CVD) by controlling parameters such as temperature and atmosphere. High crystallinity and limited defects of ultrathin 2D nanomaterials are normally produced.

In summary, it is especially important to explore advanced synthetic methods to obtain emerging 2D MOXs with desired morphology and properties. In this part, we focused on the latest advancements in the bottom-up synthesis of 2D MOXs, including optimized wet chemical synthesis, template-assisted synthesis, and vapor-phase deposition synthesis. In the wet chemical synthesis section, we specifically focus on hydrothermal/solvothermal synthesis and self-assembly synthesis. Moreover, in the template-assisted synthesis section, the 2D template and salt template methods are introduced emphatically. Finally, CVD becomes the main focus in the vapor-phase deposition synthesis section. Meanwhile, the corresponding synthetic mechanism, advantages, and limitations of the above methods are also discussed in detail.

Wet chemical method

In this section, we discuss wet chemical synthesis including hydrothermal/solvothermal synthesis and self-assembly synthesis. The basic principle of the above methods, the influence of the key parameters in the preparation process on the synthesis of 2D MOXs, and the latest research progress on MOXs are introduced in detail.

Hydrothermal/solvothermal synthesis is a typical wet chemical synthesis method involving the synthesis of many 2D non-layered MOXs. The general process of hydrothermal/solvothermal synthesis of 2D MOXs is to select a suitable precursor in a sealed container and use water or solvent as the reaction medium. When the reaction temperature of the closed system is above the boiling point of the solvent system, the high temperature and pressure environment promotes the reaction in the system, and 2D nanosheets are constructed under the induction of catalysts or surfactants. Finally, ultrathin 2D metal oxide nanosheets with good crystallization are obtained after removing surfactants by filtration and centrifugation (Alli et al., 2020; Sun et al., 2014). Based on this generalized synthesis strategy, ultrathin 2D MOXs (TiO_2 [Lan et al., 2018], ZnO [Sahu et al., 2018], MoO_3 [Alsaif et al., 2014], and WO_3 [Khan et al., 2017]) have been successfully synthesized.

Moreover, Sun et al. reported that atomically thin CeO_2 sheets with surface-confined pits were prepared by a hydrothermal method combined with the subsequent thermal annealing treatment (Sun et al., 2013). Briefly, intermediate products ($CeCO_3OH$ sheets) were firstly synthesized from cerium chloride and the surfactant via the hydrothermal reaction. Then, the intermediate sheets were transformed into ultrathin CeO_2 sheets with a thickness of ~0.6 nm and surface-confined pits via the thermal annealing treatment. Gao et al. also successfully synthesized a similar 2D nanostructure by employing cerium glutamic acid hexahydrate as the precursor (Gao et al., 2021). Besides, ultrathin In_2O_3 porous sheets with rich oxygen vacancies can be successfully synthesized via the similar hydrothermal method combined with the subsequent thermal annealing process (Lei et al., 2014).

Not only the binary metal oxide nanosheets can be synthesized by the hydrothermal approach but also ternary MOXs nanosheets can be synthesized. Yang et al. reported that the spinel-type 2D metal oxide nanosheets (γ-Ga_2O_3, $ZnGa_2O_4$, and $MnGa_2O_4$) can be prepared by the hydrothermal reaction process (Yang et al., 2019). Figure 3A describes the schematic process of hydrothermal reactions for the growth of spinel-type metal oxide nanosheets. In a typical synthetic process, $Ga(NO_3)_3$ and $M(CH_3COO)_2$ (M = Zn and Mn) are used as a source of Ga and M anions, while H_2O and ethylenediamine (EDA) with an optimized volume ratio of 2/1 were employed as the solution. The whole hydrothermal reaction is carried out in a well-sealed autoclave heated at 180°C and lasts for 24 h. It is worth noting that during the initial nucleation of the γ-Ga_2O_3 or M-doped γ-Ga_2O_3 nanosheet (Figure 3B, stage I), nucleated nanosheets tend to self-assemble into nanoflowers/clusters to decrease the large surface energy and instability induced by a large number of dangling bonds on the surface. Di et al. firstly prepared the ultrathin layered BiOBr nanosheets by employing the surfactant polyvinylpyrrolidone (PVP)-assisted hydrothermal method (Di et al., 2018).

Whereafter, the ultrathin Bi_2WO_6 nanosheets can be obtained via the ion exchange process by using pre-prepared atom-thick BiOBr nanosheets as the precursors (Figure 3C). Based on this strategy, 2D Bi_2MoO_6 nanosheets were also prepared successfully (Di et al., 2019).

In summary, the hydrothermal/solvothermal synthesis method is a simple, low-cost, and scalable method for the synthesis of ultrathin 2D MOXs. However, it is hard to figure out the growth mechanism of the hydrothermal/solvothermal synthesis process as the reactions take place in a sealed autoclave. This makes it difficult to design experimental schemes for synthesizing other 2D MOXs. In addition, the hydrothermal/solvothermal synthesis is sensitive to experimental conditions such as the concentration of precursors, solvent systems, employed surfactants or polymers, and temperature, thus making it difficult to precisely control the structure or morphology repeatedly. Furthermore, most of the 2D nanosheets synthesized by the hydrothermal/solvothermal synthesis method were few-layer or few-unit-cell thick while single-layer or single-unit-cell thick was rarely found (Liu et al., 2015).

Self-assembly is often combined with the hydrothermal/solvothermal synthesis of 2D MOXs. In this method, surfactants are often used as structure-directing agents to confine the stacking and growth of metal oxide along with selected directions. Figure 4A shows a schematic diagram of the self-assembly synthesis of ultrathin 2D MOXs. The metal oxide oligomers are strategically and collaboratively self-assembled into lamellar structures with polymer surfactant molecules before they are condensed, polymerized, and crystallized into atomically thin 2D metal oxide nanosheets. Whereafter, removing the surfactant templates is an essential step to obtain high-quality 2D nanosheets through intensive centrifugal filtration and subsequent washing. Based on the above surfactant self-assembly method, 2D nanostructures of some typical transition MOXs such as TiO_2, ZnO, Co_3O_4, WO_3, Fe_3O_4, and MnO_2 have been successfully prepared (Sun et al., 2014).

Recently, Zhang et al. reported a general and facile strategy for the synthesis of 2D metal oxide nanosheets induced by nonionic surfactant micelles (Zhang et al., 2019). The precursor solution for this strategy only consisted of the deionized water solvent, metal salts, and P123 (polyethylene oxide-polypropylene oxide-polyethylene oxide) nonionic surfactants, while the synthesis process was mainly based on the thermo-regulated phase transition of the micelles. Specifically, when the temperature of the surfactant solution rises, the surfactants can transform into monodisperse molecules, spherical micelles, and lamellar micelles along with the temperature of the surfactant solution ranging from 0°C to 50°C (Figure 4B). The formed lamellar micelles constituted a quasi-2D confined space, which can be filled with an aqueous solution containing metal ions, thus forming layered metal hydroxides through rapid hydrolysis. Furthermore, high-temperature treatment not only led to the growth and crystallization of metal hydroxides but also converted the metal hydroxides to the corresponding 2D MOXs nanosheets. With this method, various kinds of high-quality 2D MOXs were successfully synthesized, which include six transition metal elements from VIIB to IIB (Mn_3O_4, Fe_2O_3, CuO, NiO, and ZnO) and two main groups of elements (SnO_2 and Sb_2O_3). Owing to the high specific surface area and enhanced surface activity, 2D mesoporous metal oxide presented excellent potentials in catalysts, batteries, sensing, and energy-related applications. Lan et al. successfully synthesized a new type of 2D single-layer mesoporous TiO_2 nanosheets with very uniform size and thickness as well as ordered mesostructure via a hydrothermal-induced solvent-limited assembly method (Lan et al., 2018). In particular, the prepared precursor solution contained the solvent tetrahydrofuran (THF), which evaporated at a low temperature of ~45°C, resulting in the precursor solution turning into a viscous gel. The gel was then dispersed in mixed solvents of ethanol and glycerol, followed by hydrothermal treatment at 100°C. It is worth noting that the assembly process of mono micelles takes place entirely under the guidance of surrounding glycerol in a spatially confined 2D direction without using any solid interfaces. In conclusion, self-assembly is a general method to synthesize many 2D MOXs, which presents the advantages of simplicity and efficiency. However, there are challenges in accurately controlling the thickness and lateral size of the nanosheets, which are similar to those faced by the hydrothermal/solvothermal approaches.

Template-assisted method

Template-assisted synthesis is an effective strategy for the growth of anisotropic nanostructures, which refers to the use of pre-synthesized nanomaterials or bulk substrates as templates to confine/direct the growth of specific nanostructures. For the synthesis of 2D MOXs, the selection of the template is of crucial importance as the assembly of nanocrystals should be limited within a 2D confined space and the growth

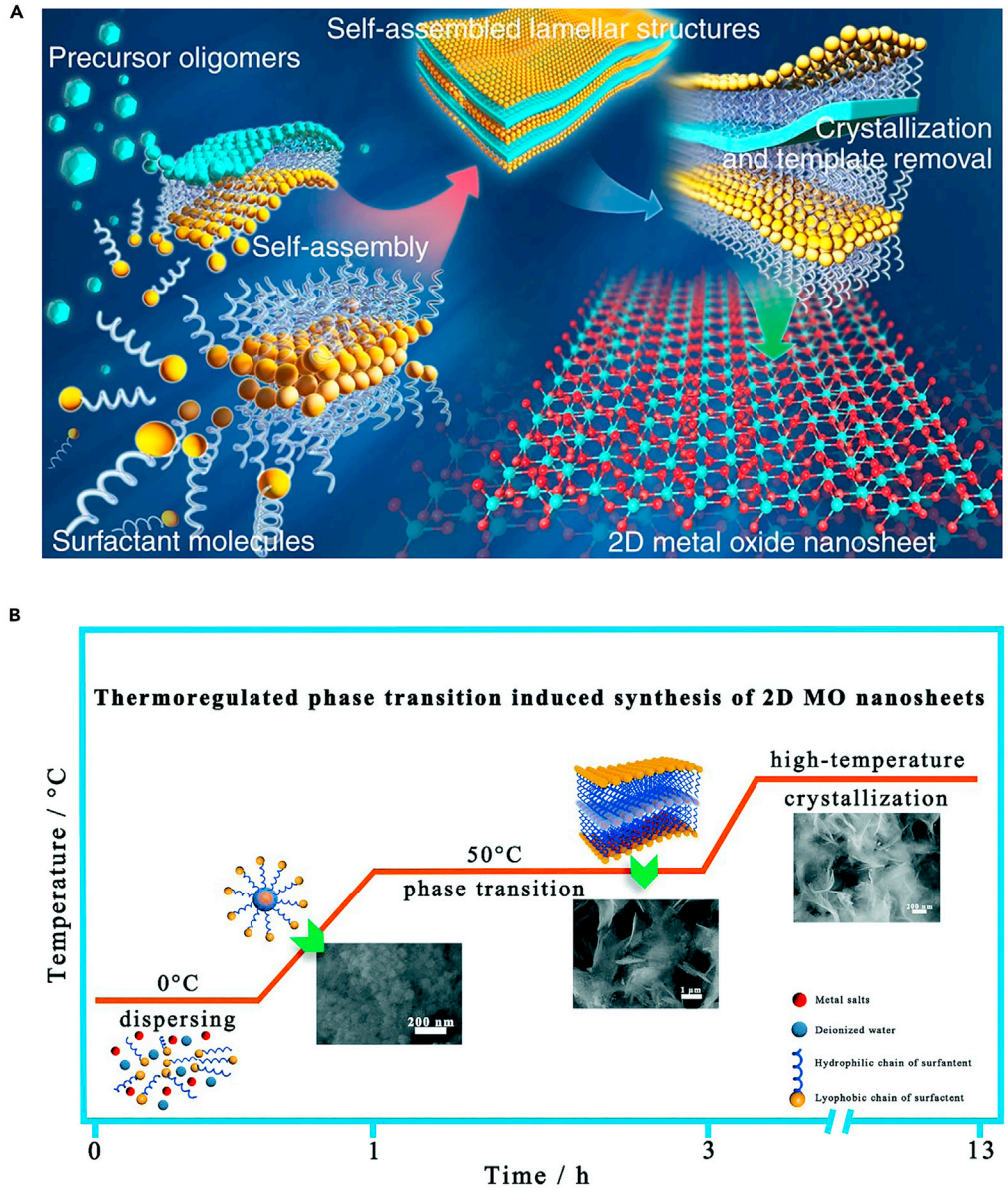

Figure 4. Bottom-up synthesis: self-assembly synthesis of 2D MOXs

(A) Schematic illustration for the self-assembly of 2D metal oxide nanosheets (Lei et al., 2021) Copyright 2021, Elsevier.
(B) Schematic illustration for the synthesis of 2D metal oxide nanosheets based on the thermo-regulated phase transition (Zhang et al., 2019) Copyright 2019, Royal Society of Chemistry.

along the third dimension must be retarded. Hereinto, alternative 2D templates can be classified into soft and hard colloidal templates. The soft template method, which uses surfactant micelles as the structure-directing agents, has already been included in self-assembly, oriented attachment, and lamellar intermediate-assisted exfoliation methods. Therefore, this section is primarily focused on the synthesis of 2D MOXs using 2D hard templates (such as graphene oxide (Cao et al., 2015), graphitic carbon nitride nanosheets (Xu et al., 2019), Li_2O_2 nanosheets (Xue et al., 2020), and salt templates (water-soluble salts)) as the growth templates. Moreover, the latest studies will be summarized and the basic composition strategies, fundamentals, advantages, and challenges of the template-assisted synthesis will be also reviewed.

Graphene oxide (GO) is a typical 2D template as it possesses a large amount of oxygen-containing functional groups and shows a strong affinity towards inorganic materials (Takenaka et al., 2015). In addition,

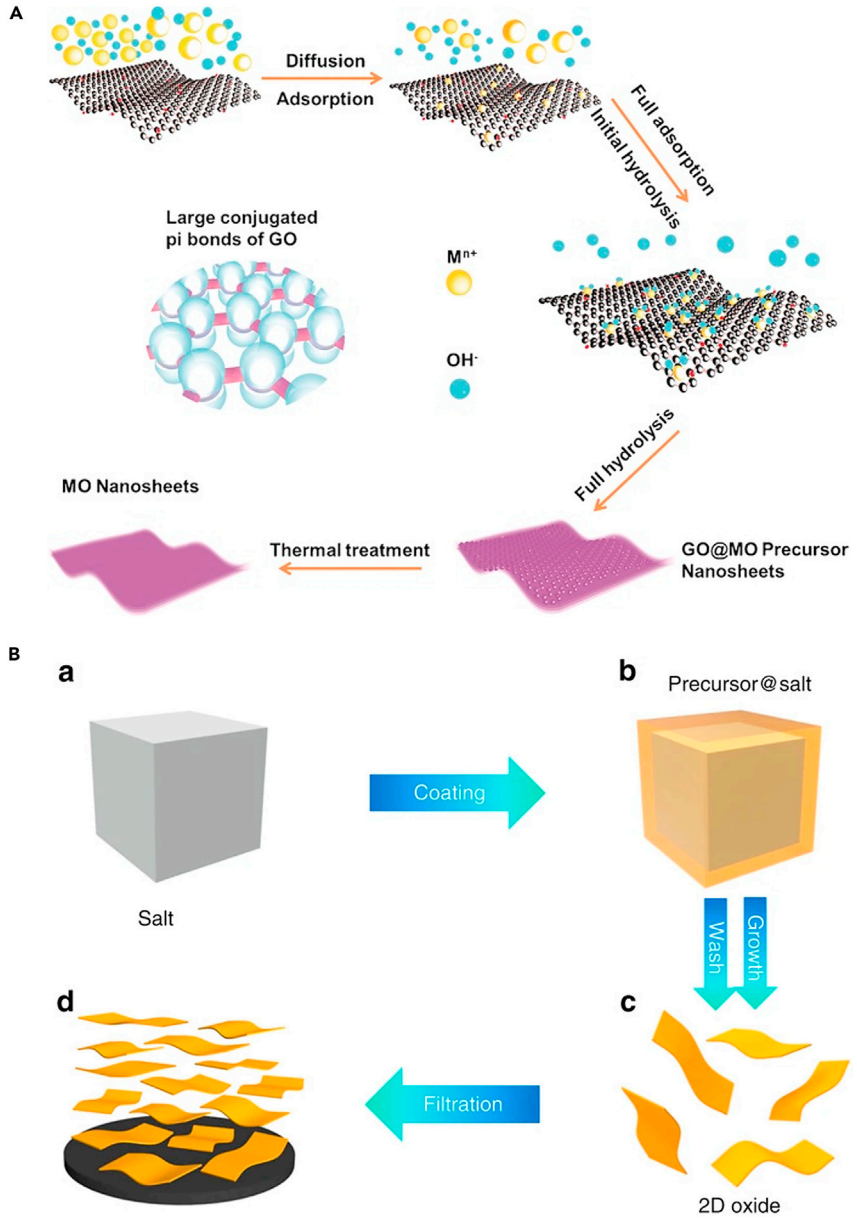

Figure 5. Bottom-up synthesis: template-assisted synthesis of 2D MOXs

(A) The strategy for the synthesis of large-size ultrathin 2D MOXs by GO template (Zhao et al., 2021a) Copyright 2021, John Wiley and Sons Ltd.

(B) Schematic diagram of 2D MOXs synthesis by salt template method (Xiao et al., 2016) Copyright 2016, Springer Nature.

it is highly dispersible in the solvent that could direct the growth of ultrathin nanosheets with high throughput. Huang et al. successfully synthesized γ-Al_2O_3 nanosheets (~4 nm) by duplicating the shape of GO (Huang et al., 2016). In detail, a continuous and uniform amorphous basic aluminum sulfate (BAS) layer was firstly coated on the surface of GO through precipitation from a homogeneous solution. After calcinating at 800°C, GO was removed from the composite while the BAS layer was converted into a 2D Al_2O_3 nanosheet, which presented the lateral size of tens of microns and thickness of about 4 nm.

By using GO as the template in a wet chemical system, Zhao et al. reported a generalized and facile strategy to synthesize the large-size ultrathin 2D MOXs with the thickness at several nanometers (Zhao et al., 2017). As the schematic is shown in Figure 5A, the large π bond on the GO surface and the electrostatic

adsorption of metal cations can make the metal cations firmly adsorb on the GO surface. Then, by precisely controlling the temperature and pH of the liquid-phase reaction, the controlled hydrolysis of the metal cation was promoted to achieve a balance between the nucleation and growth of the metal cation on the GO surface. Finally, the GO@MO precursor composites were thermally treated (650°C for 2 h), during which GO was removed and ultrathin 2D MOXs were obtained. Notably, such a strategy mainly relies on the accurate control of the balance between the heterogeneous growth and nucleation of MOXs on the surface of GO, which was independent of the individual character of the metal elements. Therefore, ultrathin nanosheets of various MOXs, including those from both main-group (MgO, Al_2O_3, SnO_2, and Sb_2O_5) and transition elements (ZrO_2 and TiO_2) were successfully synthesized that demonstrated the strong universality of this method. Besides, as the lateral size of the ultrathin 2D metal oxide nanosheets is determined by that of GO, this approach is also a feasible way to synthesize large-size metal oxide nanosheets as GO can be easily produced up to dozens of micrometers. More importantly, the thickness of the 2D MOXs can be also adjusted by controlling the concentration of the metal salts in the solutions.

In addition to the 2D templates, the salt crystal surface can also provide a template for the growth of 2D MOXs. In most cases, the salt is water-soluble and can be easily removed by the subsequent process. Xiao et al. reported a general strategy that used the surface of water-soluble salt crystals as growth templates and it was not only applied to the layered MOXs but also various non-layered MOXs (including hexagonal MoO_3, MoO_2, MnO, and hexagonal WO_3) (Xiao et al., 2016). Taking the synthesis of MoO_3 or WO_3 as an example, a molecular precursor solution was firstly prepared (Mo powder or W powder was dispersed in ethanol and added to H_2O_2) and mixed with a large volume of inorganic salt (NaCl or KCl) to form precursor@salt. Next, the solution was dried and the mixture was annealed at an elevated temperature. Finally, after washing and filtration, 2D MoO_3 or WO_3 nanomaterial was obtained with a large lateral size (up to 100 μm) (Figure 5B). Generally, the growth of 2D MOXs was promoted by the lattice matching between the salt surface and target production. The thickness of the 2D MOXs was controlled by mixing a limited volume of the dilute oxide precursor solution with a large number of salt microcrystals. Based on the above standard strategy, α-Fe_2O_3 (Mohiuddin et al., 2020) and SnO_2 (Gu et al., 2019) have been also successfully synthesized.

In summary, both the 2D template method and salt template method have advantages of low cost, high yield, and controllable morphology. At the same time, the method is universal and can be extended to other non-layered 2D MOXs also. Nevertheless, there are still several challenges, such as the relatively high cost of templates, efficient template removal, and the recycling of templates.

Vapor-phase deposition method

The vapor-phase deposition is another option for the controllable preparation of high-quality ultrathin 2D MOXs. In this section, various vapor-phase deposition for the preparation of 2D MOXs are discussed, those include chemical vapor deposition (CVD), pulsed laser deposition (PLD), and atomic layer deposition (ALD).

Among the aforementioned vapor-phase deposition synthesis methods, CVD has been continuously developed and recognized as one of the most reliable and powerful techniques for producing a large number of ultrathin 2D nanomaterials (Zhao et al., 2019; Tong et al., 2019). In general, the CVD method to grow the 2D nanomaterials involves three essential steps, which include evaporation and thermal decomposition of precursors, transport and migration of reactants, as well as the nucleation and growth of crystals on the substrate. By fine-tuning, the involved experimental parameters, such as precursors, substrates, catalysts, temperature, and atmospheres, the controllable growth of 2D nanomaterials with tunable layer number (or thickness), crystallinity, and exposed crystal facets can be achieved (Qin et al., 2020; Yu et al., 2015).

Guo et al. reported that the 2D vertical heterostructures of MoO_3-MoS_2 were successfully synthesized on SiO_2/Si substrates via a one-step CVD process (Figure 6A) (Guo et al., 2021). At the fixed reaction temperature (720°C), different products can be obtained by changing the location of the sulfur source to adjust the concentration of sulfur vapor. The MoS_2 nanosheets can be synthesized when S powder is 15 cm away from MoO_3 precursors, while MoO_3 nanosheets can be synthesized due to the shortage of sulfur atoms when S power is more than 19 cm away from MoO_3 precursors, and its thickness increased with temperature. In addition, the vertical heterostructures can be synthesized in the middle-state. Kim et al. successfully synthesized wafer-level α-MoO_3 on a Si/SiO_2 at a low temperature of 150°C by using an inductively coupled plasma-enhanced CVD system (Kim et al., 2017). The mechanism for the synthesis of wafer-scale MoO_3

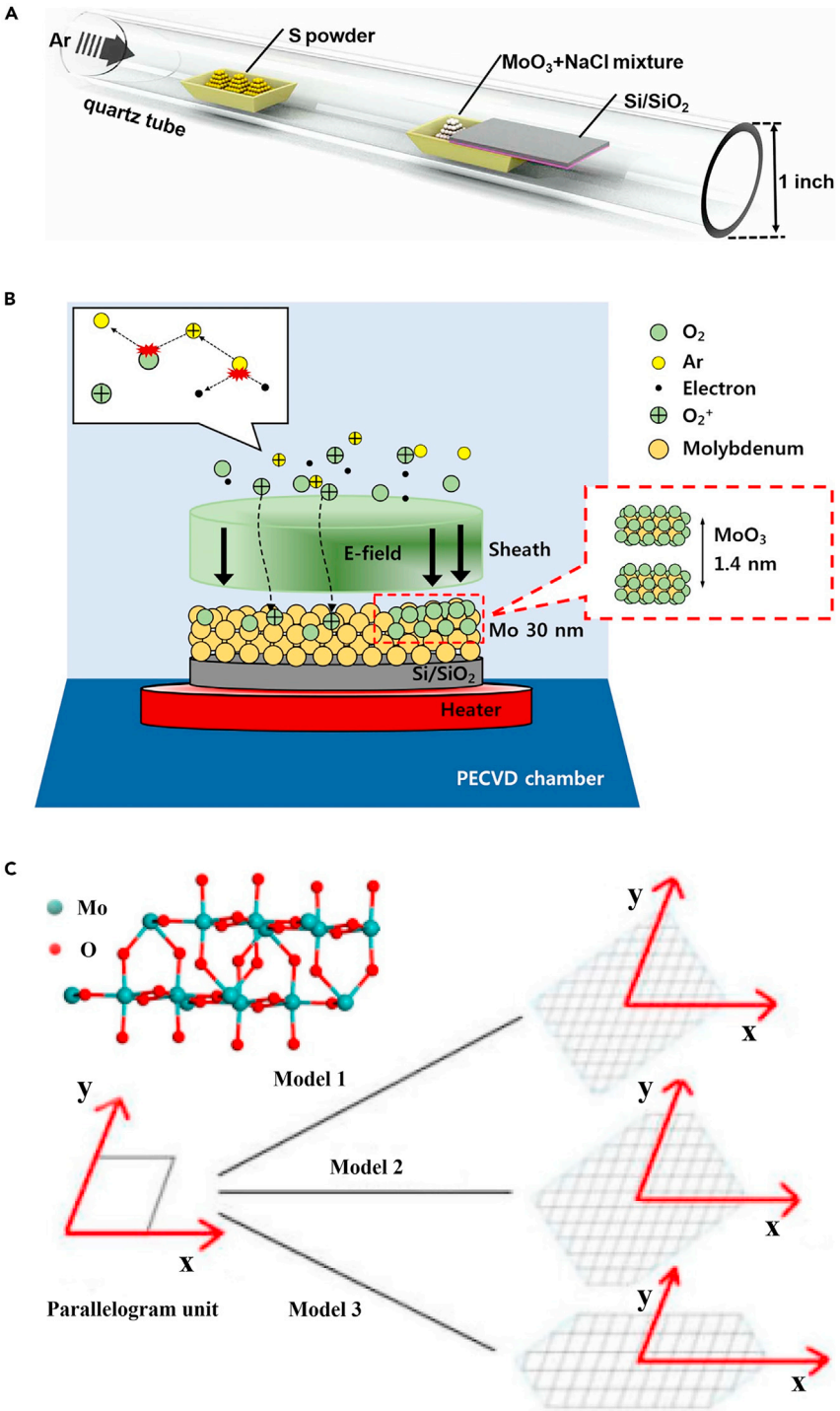

Figure 6. Bottom-up synthesis: CVD synthesis of 2D MOXs

(A) The set-up diagram for the synthesis of MoO_3-MoS_2 heterostructures (Guo et al., 2021) Copyright 2021, IOP Publishing Ltd.

(B) Schematic for the synthesis of MoO_3 on Si/SiO_2 (Kim et al., 2017) Copyright 2017, IOP Publishing Ltd.

(C) The schematic of three growth models of 2D MoO_2 and their corresponding atomic structure was constructed with the thinnest plane (020) (Luo et al., 2020) Copyright 2020, Elsevier BV.

is illustrated in Figure 6B. During the plasma activation, the Ar gas in the chamber was ionized. Herein, the specific reason to use Ar is to produce more oxygen ions in the sheath area of plasma, thus assisting the penetration of O_2 plasma into the 30 nm thick e-beam evaporator-deposited Mo film to produce the 2D MoO_3.

By employing the CVD technique, not only layered 2D MOXs but also non-layered 2D MOXs can be facilely prepared. For example, Lee et al. successfully synthesized 2D TiO_2 nanosheets with high-density anatase via a CVD process, in which $TiCl_4$ was employed as the precursor and the mixture gas of oxygen and argon are used as the reaction gases (Lee and Sung, 2012). This method yielded TiO_2 nanosheets on a silica substrate, which possessed high-energetic exposed facets of (001), thus presented more active characteristics thermodynamically and making it highly suitable for various applications. Recently, Luo et al. reported that the micrometers-scale 2D MoO_2 single crystals with a thickness of ~3.8 nm can be synthesized by reducing the MoO_3 via hydrogen in the atmospheric pressure CVD (Luo et al., 2020). It is worth mentioning here that the shape of 2D MoO_2 single crystals had three types, including the standard parallelogram, the parallelogram with two angles missed, and the hexagonal. Here, a similar growth velocity along the x-axis is the same (Figure 6C), while the growth velocity along the y-axis is different. Therefore, the difference in growth velocity between the y-axis and the x-axis is the key factor that decides the final shape of 2D MoO_2.

In general, 2D nanomaterials synthesized by the CVD method are based on stiff solid substrates with a large number of crystal defects randomly distributed on the surface, resulting in the stochastic nucleation of 2D nanomaterials and relatively low mass transfer efficiency. Moreover, because the subsequent growth of 2D nanomaterials after nucleation continues at the fixed initial nucleation sites, the self-assembly of grains grown on solid substrates is almost impossible. The resulting material usually exhibits an inhomogeneous number of layers and is composed of small domains and massive grain boundaries, resulting in large variations from theoretical expectations (Zhang and Fu, 2018). In recent years, the liquid metal CVD strategy for the controllable fabrication of 2D nanomaterials is proposed. The self-limited growth of 2D nanomaterials can be triggered by utilizing the phase transition of liquid metals, leading to the synthesis of a strictly uniform monolayer. In addition, excellent rheological properties of liquid metal can be used to effectively achieve artful self-assembly (Zeng and Fu, 2018).

Yang et al. presented an approach to synthesize high-quality ultrathin antimony oxide single crystals via a substrate-buffer-controlled CVD strategy (Yang et al., 2020a). Firstly, a high-temperature (1000°C) annealing process was employed to prepare a resolidified Ag (111) substrate. Then, antimony powder was used as the antimony source to provide antimony vapor and carried downstream by the mixture of Ar, H_2, and O_2. Subsequently, Sb atoms react with O_2 to grow ultrathin antimony oxide single crystals on the substrate (Figure 7A). Owing to the reaction, Gibbs free energy of Sb with O_2 ($-110.97\ kJ\cdot mol^{-1}$) is much lower than that of Ag ($-7.84\ kJ\cdot mol^{-1}$), Sb reacts preferentially with oxygen. However, the amount of O_2 must be limited to avoid oxidation of the Ag substrate while the amount of elementary Sb should be controlled to achieve the complete oxidation of Sb to form an ultrathin antimony oxide single crystal. Here, the Ag substrate served as a buffer to achieve a modest supply of Sb. When excessive Sb was present on the substrate, the buffer effect of the Ag substrate kept Sb at a constant throughout the Ag substrate, which was essential for the complete oxidation of antimony and the subsequent growth of ultrathin antimony oxide crystals. In addition, Li et al. successfully synthesized 2D rare-earth oxides (REO) single crystal by using the above strategy (Li et al., 2021b). Besides, it is still a great challenge to obtain 2D single crystals with specific crystal facets for REO due to their intrinsic non-layered structure and disparate thermodynamic stability of different facets. During the CVD growth process of 2D REO single crystal, the strong interaction between the introduced facet-controlling assistor (FCA. By employing NH_4X ($X^- = Cl^-$, Br^-, I^-) as FCA, it is easy to provide active assistor X ions (base) to assist single crystal growth) and the REO surface greatly manipulates the growth mode and direction of non-layered REO. The introduction of FCA not only suppresses isotropic growth along the 3D direction and impedes the thickening of 2D REO but also causes the relative surface energy (γ) of each facet to change with increasing concentration of FCA (Figure 7B). This strategy can be extended to a series of planar controlled syntheses of 2D REO single crystals, including light REO (CeO_2 and Nd_2O_3), middle REO (Sm_2O_3 and Eu_2O_3), and heavy REO (Dy_2O_3, Ho_2O_3, and Y_2O_3).

In summary, CVD is still mainly used for the preparation of layered chalcogenide, graphene, boron nitride, etc. while there are still few cases for 2D MOXs (both layered and non-layered) (Yang et al., 2017b; Yu et al., 2015). The successful synthesis of a high-quality single crystal of REO by liquid CVD strategy is not only an

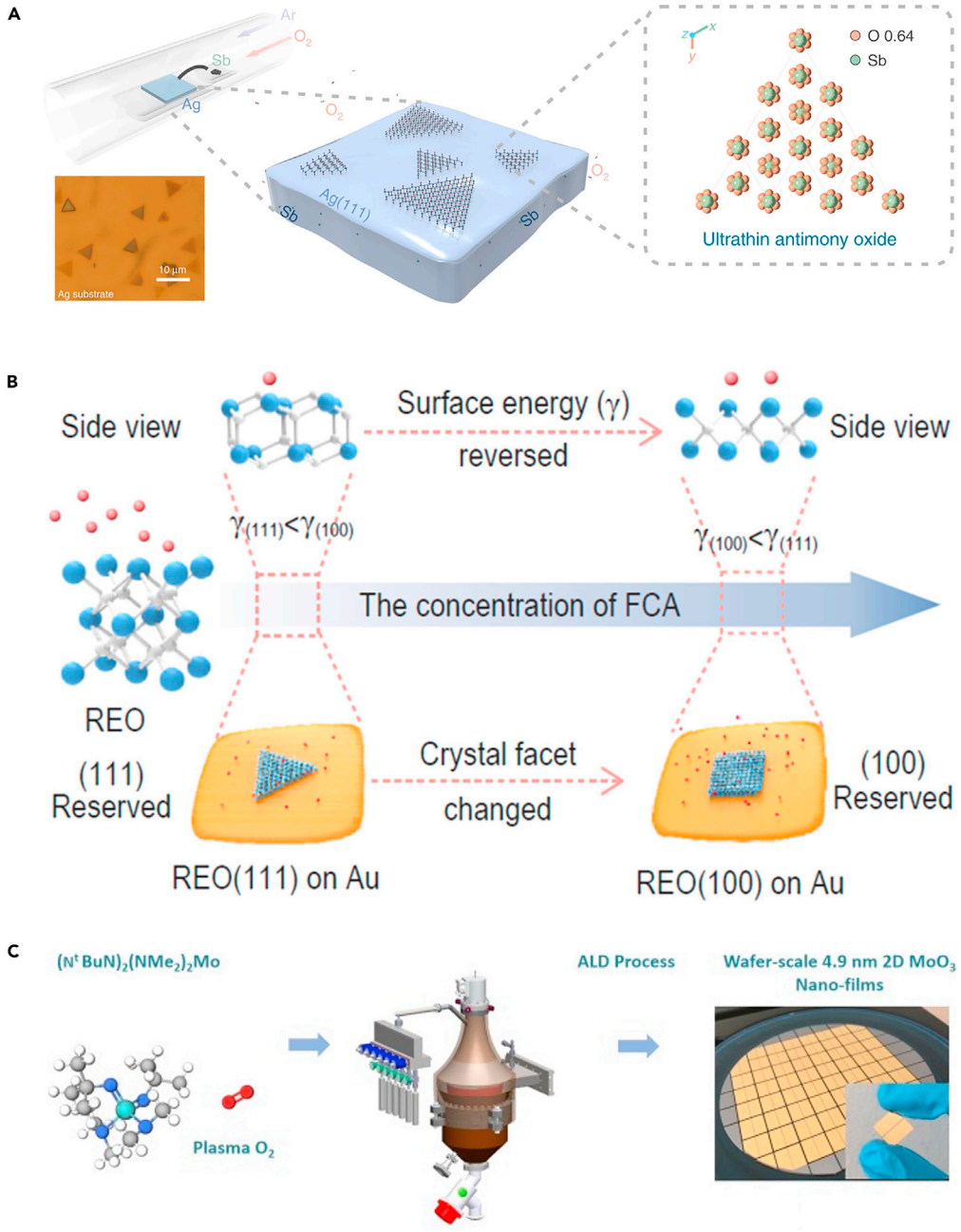

Figure 7. Bottom-up synthesis: liquid metal-assisted CVD strategy and ALD synthesis of 2D MOXs

(A) The schematic for the growth of ultrathin antimony oxide on the resolidified Ag substrate and related optical microscope image (Yang et al., 2020a) Copyright 2020, Springer Nature.

(B) Schematic illustration of the facet-controllable synthesis strategy assisted by the FCA (blue atoms, RE atoms; white atoms, O atoms; red atoms, X ions) (Li et al., 2021b) Copyright 2021, Oxford University Press.

(C) The schematic to prepare the 2D α-MoO_3 nanofilms via the ALD method (Wei et al., 2018) Copyright 2018, Elsevier.

important supplement to CVD but also of great significance for the application of REO. Additionally, space-confined CVD is another potential strategy for preparing 2D MOXs, in which growth space is constrained into 2D or 3D form to improve the controllability of the synthesis process and reduce the thickness of the products and the nucleation density on the substrate. Therefore, the large area growth of high-quality and homogeneous 2D materials is conducive (Zhou et al., 2018).

Table 2. The summary of the bottom-up synthesis for the fabrication of 2D MOXs

Synthesis methods	Advantages	Limitations	Materials	Thickness (nm)	Applications	Ref.
Hydrothermal/Solvothermal synthesis	Simple Low cost Scalable	Poor repeatability	CeO_2	0.6	Photocatalyst	(Gao et al., 2021)
Self-assembly	Low cost Scalable	Residual	WO_3	2.1	Photodetector	(Sun et al., 2014)
			TiO_2	0.62	Photodetector	(Sun et al., 2014)
Template-assisted	High yield Low cost	Residual	Al_2O_3	4	Catalyst	(Huang et al., 2016)
			MgO	3.6	Electronic devices.	(Zhao et al., 2017)
CVD	High controllability High quality	High cost	MoO_2	3.8	Electronic device	(Luo et al., 2020)
			SbO_2	1.8	–	(Yang et al., 2020a)
PLD	High quality	High cost	α-MoO_3	6	Gas sensor	(Bisht et al., 2021)
ALD	High controllability High quality High yield	High cost	MoO_3	4.9	Electrochemical sensor	(Wei et al., 2018)

In addition to CVD, the preparation of 2D MOXs by PLD and ALD has also made important progress. Recently, Bisht et al. successfully fabricated 2D α-MoO_3 by PLD using laser energy to deposit sintered solid MoO_3 on a substrate (Bisht et al., 2021). The thickness of obtained 2D α-MoO_3 was thinner than previously reported by the CVD method, but its lateral size was less than 1 μm, which greatly limited its application especially in high-performance electronic devices. Furthermore, Wei et al. successfully prepared 2D α-MoO_3 nanosheets with a thickness of ~4.9 nm by ALD as a variant of CVD (Wei et al., 2018). In this work, a cross-flow reactor was firstly used with $(N^tBuN)_2(NMe_2)_2Mo$ and oxygen plasma gases as molybdenum precursor and oxygen precursor, respectively. 2D α-MoO_3 nanofilms after the optimizing deposition temperature, pulse duration, and purge time parameters were then obtained on SiO_2/Si wafers as shown in Figure 7C. ALD technology is a surface-controlled layer-by-layer process based on self-limiting chemical reactions and has the advantage of depositing large-scale conformal dense nanofilms with precise thickness and component control at relatively low temperatures (less than 350°C). However, the lateral size of nanosheets obtained by this method is relatively small and there are challenges in preparing non-layered 2D MOXs.

At the end of the bottom-up synthesis section, the listed Table 2 not only summarizes the advantages and limitations of various synthesis methods but also summarizes the thickness and application of the synthesized 2D MOXs.

Liquid metal strategy

Although several methods can synthesize the 2D MOXs, their large-scale production under the requirements of low cost, high yield, and maneuverable are still full of challenges. Recently, the emerging liquid metal method provided an effective solution to the above problems. More importantly, such methods are particularly suitable for the synthesis of non-layered MOXs.

Liquid metals have traditionally been defined as metals and alloys whose melting points are close to or below room temperature (Zhang et al., 2014, 2015). Mercury (Hg) and gallium (Ga) are two typical liquid metals at room temperature, while the potential hazards of mercury make it unusable in many applications. In addition, some metals such as indium (156°C) or tin (231°C) have significantly lower melting points than ordinary metals, which are also considered to be within the category of liquid metals. Moreover, some eutectic alloys with low melting points are also included, such as gallium-based eutectic alloys (EGaIn - eutectic gallium-indium binary alloy [Wang et al., 2020]), galinstan (i.e. gallium-indium-tin ternary alloy), and doped metals (e.g. the In-Sn alloys with Sn concentrations between 0 and 20 at %) (Kalantar-Zadeh et al., 2019).

Owing to amorphous structure, electron-rich "sea" and abundant vacancies within the bulk, liquid metals present special properties, including good solubility, chemical reactivity, and weak interfacial forces, which are the

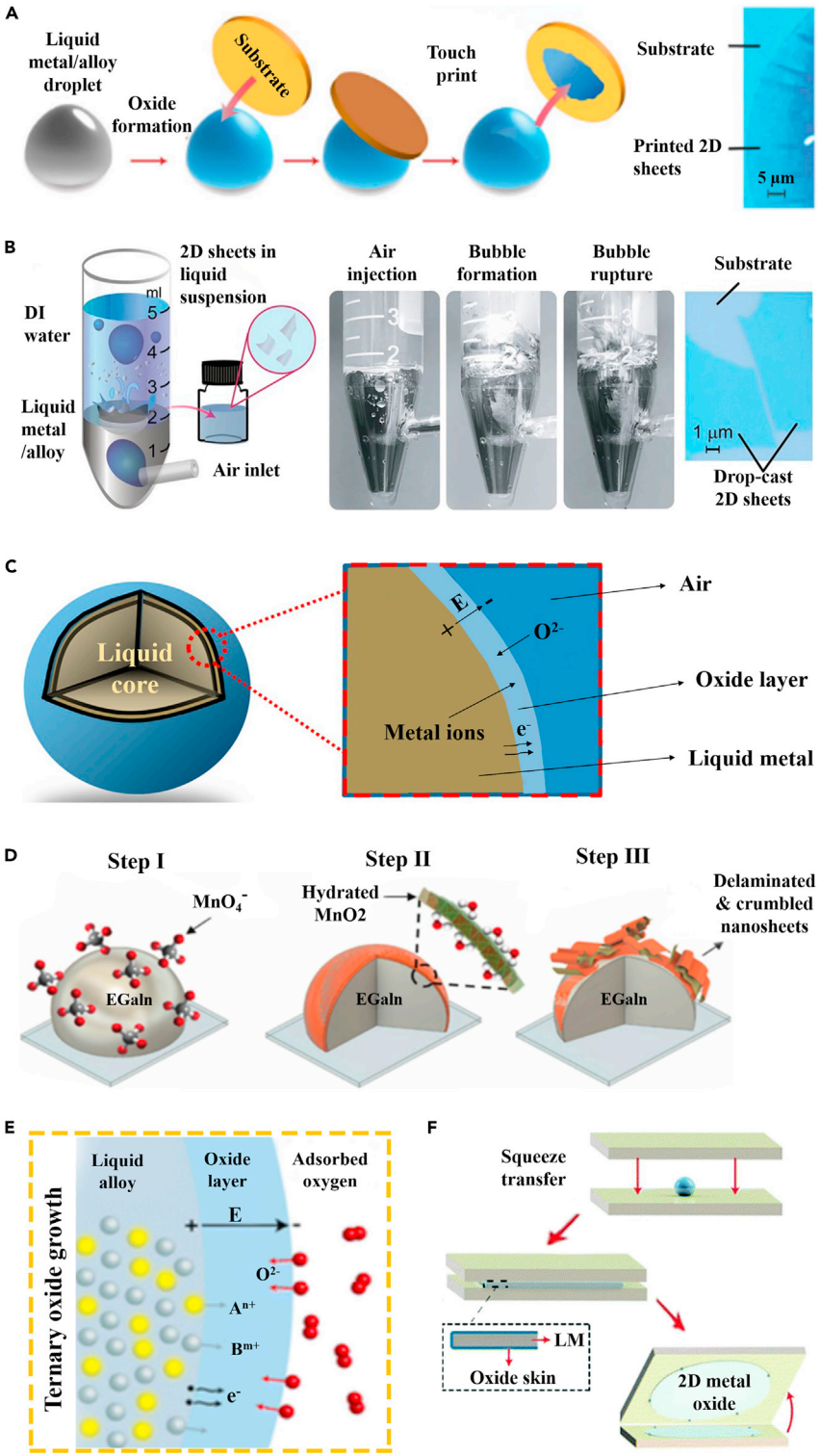

Figure 8. Liquid metal strategy: the schematic to prepare 2D MOXs by three generations liquid metal methods

(A) The schematic to prepare the ultrathin 2D MOXs by touch printing on the liquid metal or alloy surface (Zavabeti et al., 2018) Copyright 2018, American Chemical Society.

(B) The schematic of the gas injection method (Zhao et al., 2021b) Copyright 2021, Tsinghua University Press.

Figure 8. *Continued*

(C) The growth mechanism of an oxide skin that described by the Cabrera–Mott model (Goff et al., 2021) Copyright 2021, Royal Society of Chemistry.

(D) The formation process of the hydrated MnO2 on the surface of EGaIn in an aqueous KMnO4 solution (Ghasemian et al., 2019) Copyright 2019, Wiley-VCH Verlag.

(E) Schematic illustration of ternary oxide growing on the liquid alloy surface.

(F) Schematic illustration of the squeeze printing process (Shi et al., 2021) Copyright 2021, Springer Nature.

theoretical basis as the host for the synthesized 2D MOXs (Zhao et al., 2021b). The presence of vacancies endows liquid metals with the ability to accommodate heteroatoms. For example, Ga with a small radius can diffuse into the lattices of other metals. In addition, due to the wide melting range of liquid metals, they can dissolve or disperse most metals to form eutectic alloys or doped metals. Thereinto, the eutectic alloys or doped liquid metals are prepared by combining two or more metals in a specific composition at a certain temperature, which usually exhibits lower melting points than that of monoelemental metal. Compared with the bulk, the interatomic interaction near the surface of liquid metals is more active, resulting in unique properties and hence providing opportunities for chemical reaction at the interfaces between the liquid metals and the surrounding environments. Liquid metals possess chemically active surfaces due to their low potential, in which the simplest and the most widespread reaction occurs with oxygen to form an ultrathin and native oxide skin on the metal surfaces. In addition, the feature of high electrical conductivity makes them suitable for the electrochemical redox process, presenting another approach for fabricating 2D nanostructure derived from the liquid metal host (Lertanantawong et al., 2018). In the specific atmosphere, the liquid metal owns an ultrathin skin formed at the metal-air interface, constituting a natural 2D planar structure. It is worth noting that this 2D ultrathin skin coheres to the parent liquid metal weakly, resulting in the high possibility of the delamination of the skin from the liquid metal surfaces.

Based on recent reports, we classify the liquid metal-based synthesis approaches of 2D MOXs into three generations, which are based on monoelemental metals, eutectic alloys, and doped metals. When the melted monoelemental metal is exposed to an oxygen-containing atmosphere as low as a few ppm, the surface of the liquid metal rapidly forms an oxide skin, which is considered to be a natural ultrathin 2D oxide layer. Owing to the weaker interactions between the liquid metal and its skin than that between the substrate and the skin, the ultrathin oxide skin can be exfoliated by contacting the liquid metal droplet with a target substrate (Figure 8A). Another method involves the gas injection into the liquid metal, where the interfacial oxides form at the bubble interface and the density gradients carry the oxide nanosheets into the solvent reservoir (DI water) that is placed above the molten metal (Figure 8B) (Hu et al., 2021). And then, the obtained aqueous suspension is drop-casted onto the substrate for subsequent treatment steps. Moreover, the transient growth process of oxide skin can be described by the Cabrera–Mott model (Goff et al., 2021), as shown in Figure 8C. On the one hand, owing to the electron tunneling effect, electrons escape from the liquid core and transfer to the adsorbed oxygen, thus ionizing the adsorbed oxygen and generating an electrostatic potential (Mott potential) among the interface of the oxidant-oxide and the oxide metal. The generated electric field significantly reduces the energy barrier of metal ion diffusion toward the free interface and promotes the growth of the oxide skin. On the other hand, with the prolonged oxidation time, the thickness of the oxide skin reaches a critical value (typically less than a few nanometers) and then the subsequent growth is inhibited, leading to self-limiting oxidation. For example, liquid Ga establishes a uniform and relatively dense atomically thin oxide layer in a self-limiting reaction when exposed to an oxygen-containing atmosphere (Carey et al., 2017; Li et al., 2021a). Nevertheless, some other liquid metals (e.g. tin, indium, and bismuth) exhibit a non-self-limiting oxidation process, as the formation of a porous oxide layer on the surface does not prevent further oxidation of the liquid metal. For instance, SnO is initially formed on the surface of Sn and SnO_2 begins to appear as oxidation continues (Atkin et al., 2018). However, 2D SnO nanosheets with a thickness of ~0.6 nm were synthesized at a low oxygen environment (e.g. 10–100 ppm of O_2) (Daeneke et al., 2017). Therefore, for the liquid metal with a non-self-limiting reaction, precisely controlling the oxygen content and adjusting the oxidation time of the liquid metal may lead to a surface layer with a specific thickness and surface composition. Various 2D MOXs (Bi_2O_3 (Messalea et al., 2018), In_2O_3 (Alsaif et al., 2019a), ZnO (Mahmood et al., 2021), and PbO (Ghasemian et al., 2020)) were successfully obtained based on the Cabrera–Mott model and the exfoliation technique by printing or gas injection method.

Furthermore, a wider range of 2D MOXs synthesized from liquid eutectic alloys (e.g. EGaIn and Galinstan) can be defined as the second generation of the liquid metal method. Owing to the active chemical

reactivity on the surface of the liquid EGaIn (Hoshyargar et al., 2017; Wang et al., 2021d), Ghasemian et al. generated monolayer-hydrated MnO_2 using a galvanic replacement reaction between permanganate ions and liquid EGaIn (Ghasemian et al., 2019). As for the electrochemical mechanism of the galvanic replacement reactions, the sacrificial metal templates (Ga) are oxidized in the presence of cations of another metal (Mn) with a higher standard reduction potential. An overview of the process is provided in Figure 8D. Based on thermodynamic considerations, the oxide with the greatest reduction of Gibbs free energy (ΔG_f) dominates the surface. For galinstan, despite the presence of In and Sn, the self-limiting oxide layer is exclusively composed of Ga oxide (Wang et al., 2021c). In addition, galinstan can be used as a reaction solvent due to its good solubility. Zavabeti et al. alloyed ~1 wt % of elemental Hf, Al, or Gd into the liquid galinstan, which served as the precursors for the formation of their respective oxides (Zavabeti et al., 2017). These oxides satisfied the requirement of featuring a lower ΔG_f than gallium oxide, thus forming surface oxides (HfO_2, Al_2O_3, and Gd_2O_3) on their respective alloys, which are then exfoliated by printing or gas injection method to obtain the ultrathin 2D oxide layer (Zavabeti et al., 2018).

Finally, 2D MOXs derived from the doped liquid metals are considered as the third-generation liquid metal method, which not only further expands the range of MOXs but also creates a facile synthesis method of 2D ternary MOXs. The dopants in doped liquid metals can be both from metals and non-metals (e.g. Se), which can effectively reduce the melting point and create conditions for the synthesis of some 2D MOXs. Alkatiri et al. proposed alloying 1 wt % of micron-sized Ti powder with 30 g of liquid Ga metal by mechanical grinding (Alkathiri et al., 2020). The whole process was carried out inside an Ar glove box with very low oxygen content (<10 ppm) to reduce oxidation during the handing. When the prepared Ga-Ti alloy is exposed to air, Ti in the alloy dominates the surface oxide due to the greater oxidation energy of Ti (−944 kJ mol^{-1}) than that of Ga (−544.55 kJ mol^{-1}). The colloidal suspension containing a large number of 2D oxide nanosheets was obtained by the previously mentioned gas injection method. However, the lateral size of 2D TiO_2 is generally less than 1 μm, which limits the application range and requires further optimization. Moreover, tellurium is a metalloid of the chalcogen family with a melting point of 452°C. The interfacial oxidation of liquid Te is expected to enable the synthesis of ultrathin TeO_2 according to the Cabrera–Mott growth model. However, the required β-TeO_2 phase forms only at temperatures below 350°C, which is below the melting point of its parent metal and prevents the direct synthesis of this polymorph form. To solve these problems, the p-type β-TeO_2 nanosheets were obtained using a doped metal formed from the alloying of Te with Se (Zavabeti et al., 2021). The eutectic melt contains 5 wt % Te and 95 wt % Se and exhibits a melting point much lower than 200°C. Moreover, although the eutectic mixture was rich in selenium, the deposition 2D layer was predominantly TeO_2, which can be attributed that the Te is more oxophilic than Se, resulting in a greater reduction of the ΔG_f.

In addition to the oxides from the target metal, ternary MOXs may also be obtained when doped liquid metal as the precursor. In most cases, the surface oxides of low melting point liquid alloys (e.g. EGaIn) are mainly binary. However, Datta et al. found that In-Sn alloys were an exception and their surface oxides turned out to be In-Sn ternary compounds (Datta et al., 2020). The high solubility of Sn ions in the indium oxide host most likely explains the formation of indium tin oxide (ITO) on the surfaces of these doped liquid metals, as shown in Figure 8E. This study also found that the concentration of Sn affects the conductivity of the resulting 2D ITO. The process employed entails placing small droplets of liquid alloy onto the desired substrate, followed by squeezing with a second substrate from the top, spreading evenly the droplets to cover the entire desired area. When the two substrates are separated, the liquid droplet reverts into spherical-shaped droplets due to the high surface tension of the liquid metals, resulting in highly transparent oxide sheets on various substrates such as glasses, wafers, and polymers (Figure 8F). In this way, the lateral size of the printed ultrathin layer is controlled by changing the diameter of the doped liquid metal droplet. The electronic band structure of the In_2O_3 host is greatly changed by Sn doping, making ITO with excellent electrical conductivity and high optical transparency. Nevertheless, its electronic mobility is only one-third of that of the intrinsic In_2O_3, which greatly limits its application in the new generation of transparent electronic devices. Recently, Jannat et al. selected Zn as a dopant to prepare doped liquid metals with different concentrations (between 0 and 5 atomic %), achieving large-area 2D indium zinc oxide (IZO) by utilizing the same squeeze-printing method mentioned above (Jannat et al., 2021). The optimum electron mobility is realized in the sample with lower Zn dopant concentrations, presenting an almost 20 times improvement compared to that of pure 2D In_2O_3. On the other hand, a higher level of Zn doping may lead to the domination of the ionized impurities over grain boundary scattering, thus limiting electron transportation.

The sulfidation, nitridation, and phosphorization of 2D MOXs obtained by the liquid metal method can also transform into ultrathin metal sulfides, nitrides, and phosphides. Compared to traditional one-step

Table 3. The summary of the liquid metal strategy for the fabrication of 2D MOXs

Synthesis methods	Materials	Thickness (nm)	Lateral size (μm)	Applications	Ref.
First-generation	In_2O_3	4.5	>10	Electron devices	(Alsaif et al., 2019a)
	Ga_2O_3	~1.5	>100	Field effect transistors	(Carey et al., 2017)
	SnO	1.1	>40	Gas sensor	(Daeneke et al., 2017)
	Bi_2O_3	0.75	>10	Photodetector	(Messalea et al., 2018)
	ZnO	1.1	>100	Piezoelectric filed	(Mahmood et al., 2021)
	PbO	1	>100	Piezoelectric filed	(Ghasemian et al., 2020)
Second-generation	MnO_2	1	<1	Photocatalysis	(Ghasemian et al., 2019)
	HfO_2	0.64	>20	–	(Zavabeti et al., 2017)
	Gd_2O_3	0.51	>40	–	(Zavabeti et al., 2017)
	Al_2O_3	1.1	>20	–	(Zavabeti et al., 2018)
Third-generation	TiO_2	3	<1	–	(Alkathiri et al., 2020)
	TeO_2	1.5	>100	Transparent electronics devices	(Zavabeti et al., 2021)
	ITO	~1.5	>30	Flexible electronic devices	(Datta et al., 2020)
	IZO	~1.59	>30	Flexible electronic devices	(Jannat et al., 2021)

methods, such strategies feature higher yields, lower reaction temperatures, and larger lateral sizes. Nguyen et al. reported a two-step process combining the liquid metal method and low temperature wet chemical reaction to obtain 2D indium oxysulfide from In_2O_3 (Nguyen et al., 2021). The transformation was carried out in a solution of polysulfide radical anions, in which the replacement of oxygen atoms by sulfur atoms was promoted by highly reactive trisulfur radical anions. Compared to the liquid phase, the transformation occurs more conventionally in the vapor phase, in which In_2S_3 (Jannat et al., 2020), Bi_2S_3 (Messalea et al., 2020), Ga_2S_3 (Alsaif et al., 2019b), GaN (Syed et al., 2019), InN (Syed et al., 2019), and $GaPO_4$ (Syed et al., 2018) are successfully prepared.

In summary, the unique reaction conditions at the liquid metal interface allow the growth of 2D layered and non-layered MOXs (Table 3), which overcomes the limitations of traditional exfoliation methods. In addition, the method based on liquid metal does not require careful control of the growth conditions and has obvious advantages compared with the traditional bottom-up method. However, the liquid metal method also has some limitations. Currently, only 2D MOXs that are thermodynamically stable with liquid metal can be synthesized. In addition, the degree of crystallinity is relatively low in resulted 2D MOXs with significant portions of amorphous features and structural defects. Furthermore, 2D layers normally come with residuals of liquid metal nanoparticles, making them difficult to be implemented in practical optical and electronic devices.

PERSPECTIVE AND OUTLOOK

In summary, the synthesis approaches of various 2D MOXs were summarized and classified into the top-down, bottom-up, and as well as liquid metal-derived methods. As shown in Figure 9, the production yield and environmental impacts of the aforementioned synthetic processes are compared, in which the stability and repeatability of produced 2D oxides by each method vary greatly. Therefore, synthetic methods need to be carefully selected according to particular applications. The mechanism for each synthesis process was discussed and the corresponding advantages and limitations were concluded. While the majority of reports currently focused on non-layered 2D MOXs, the recent discovery of hexagonal layered structures in a certain number of MOXs might divert significant attention in exploring layered MOXs in the planar 2D morphology specifically using top-down approaches. In addition, the emerging liquid metal-derived synthesis method was based on the particularity of liquid metal-based chemistry, in which a variety of ultrathin 2D MOXs was realized through printing and other mechanical processes regardless of their crystal structures. However, despite the recent rapid development, critical challenges on the synthesis of 2D MOXs are presented. Firstly, the controllability of the thickness and lateral size for 2D MOXs is related low for both current top-down and bottom-up approaches. Although the liquid metal synthesis method demonstrates great potentials in producing centimeter-scale 2D MOXs with precise controlled thickness

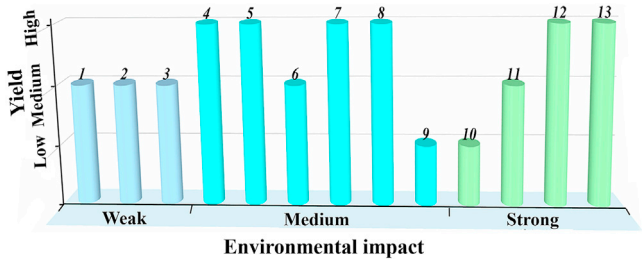

Figure 9. A comparative figure comparing the yield/environmental impacts of all synthetic processes

The numbers in the figure represent various synthesis methods, as shown below. 1, CVD; 2, PLD; 3, ALD; 4, Liquid metal strategy; 5, Template-assisted; 6, Soft chemical exfoliation; 7, Electrochemical exfoliation; 8, Ultrasonic-assisted liquid-phase exfoliation; 9, Cleavage plane-oriented exfoliation; 10, Mechanical exfoliation; 11, SC-CO_2-assisted exfoliation; 12, Hydrothermal/solvothermal synthesis; 13, Self-assembly.

owing to the self-limited oxidation behavior, the low yield, poor crystallinity, and metal contamination features hinder the practical implementation in current industries. Secondly, the emerging hexagonal layered structure is considered as the game-changer in the research field of 2D MOXs. However, its related research is still in the early stage, and the corresponding formation mechanism has not been supported by solid experimental evidence. Thirdly, to a further extent, the growth mechanisms of 2D MOXs through bottom-up approaches need to be revealed through extensive theoretical calculation and experimental supports. Particular attention should be paid to the in-depth understanding of the kinetics and directions of the 2D confined growth. Fourthly, the defect and oxygen vacancy engineering of MOXs. Fifthly, 2D multi-anionic oxygenated compound materials, including single metal oxychalcogenides (e.g. Bi_2O_2Se) (Hong et al., 2020; Wang et al., 2021a; Wei et al., 2019; Wu et al., 2017), bication oxychalcogenides (e.g. $Y_2Ti_2O_5S_2$) (Wang et al., 2019), bication oxyhalides (e.g. Bi_4NbO_8Cl, Bi_4NbO_8Br, Bi_2GdO_4Cl, Bi_2GdO_4Br, $SrBiO_2Cl$, and $PbBiO_2Br$) (Fujito et al., 2016; Kato et al., 2017; Wang et al., 2017a), bication oxynitrides (e.g. $SrTaO_2N$ and $Ca_3Nb_2N_2O_5$) (Gou et al., 2020; Wei and Xu, 2018), quinary oxychalcogenides (e.g. $Ba_2CoO_2Ag_2Te_2$) (Matsumoto et al., 2020), and quinary oxynitrides (e.g. $Li_2LaTa_2O_6N$ and $K_2LaTa_2O_6N$) (Oshima et al., 2018, 2020), enrich and develop the applications of 2D MOXs, especially in the field of photocatalysis. However, the exploration of such materials is still in their initial stage and developing controllable, facile, and low-cost preparation methods have become one of the biggest challenges.

ACKNOWLEDGMENTS

This work is supported by the National Natural Science Foundation of China (52002337, 52172155) and the Scientific and Technological Projects for Distinguished Young Scholars of Sichuan Province (2020JDJQ0028).

AUTHOR CONTRIBUTIONS

Huaguang Xie: Writing - Original Draft, Writing - Review & Editing. Zhong Li: Supervision, Writing - Review & Editing. Liang Cheng: Writing - Review & Editing. Jiaqi Tao: Writing - Review & Editing. Azhar Ali Haidry: Writing - Review & Editing. Yi Xu: Writing - Review & Editing. Kai Xu: Writing - Review & Editing. Jian Zhen Ou: Supervision, Writing - Review & Editing.

DECLARATION OF INTERESTS

The authors declare no competing interests.

REFERENCES

Aghamohammadi, H., Eslami-Farsani, R., Torabian, M., and Amousa, N. (2020). Recent advances in one-pot functionalization of graphene using electrochemical exfoliation of graphite: a review study. Synth. Met. *269*, 116549. https://doi.org/10.1016/j.synthmet.2020.116549.

Alkathiri, T., Dhar, N., Jannat, A., Syed, N., Mohiuddin, M., Alsaif, M.M.Y.A., Datta, R.S., Messalea, K.A., Zhang, B.Y., Khan, M.W., et al. (2020). Atomically thin TiO_2 nanosheets synthesized using liquid metal chemistry. Chem. Commun. *56*, 4914–4917. https://doi.org/10.1039/d0cc01456g.

Alli, U., Hettiarachchi, S.J., and Kellici, S. (2020). Chemical functionalisation of 2D materials by batch and continuous hydrothermal flow synthesis. Chem. Eur. J. *26*, 6447–6460. https://doi.org/10.1002/chem.202000383.

Alsaif, M.M.Y.A., Balendhran, S., Field, M.R., Latham, K., Wlodarski, W., Ou, J.Z., and Kalantar-Zadeh, K. (2014). Two dimensional α-MoO_3 nanoflakes obtained using solvent-assisted grinding and sonication method: application for H_2 gas sensing. Sensors Actuators, B Chem. *192*,

196–204. https://doi.org/10.1016/j.snb.2013.10.107.

Alsaif, M.M.Y.A., Field, M.R., Daeneke, T., Chrimes, A.F., Zhang, W., Carey, B.J., Berean, K.J., Walia, S., Van Embden, J., Zhang, B., et al. (2016). Exfoliation solvent dependent plasmon resonances in two-dimensional sub-stoichiometric molybdenum oxide nanoflakes. ACS Appl. Mater. Inter. *8*, 3482–3493. https://doi.org/10.1021/acsami.5b12076.

Alsaif, M.M.Y.A., Kuriakose, S., Walia, S., Syed, N., Jannat, A., Zhang, B.Y., Haque, F., Mohiuddin, M., Alkathiri, T., Pillai, N., et al. (2019a). 2D SnO/In_2O_3 van der Waals heterostructure photodetector based on printed oxide skin of liquid metals. Adv. Mater. Inter. *6*, 1900007. https://doi.org/10.1002/admi.201900007.

Alsaif, M.M.Y.A., Pillai, N., Kuriakose, S., Walia, S., Jannat, A., Xu, K., Alkathiri, T., Mohiuddin, M., Daeneke, T., Kalantar-Zadeh, K., et al. (2019b). Atomically thin Ga_2S_3 from skin of liquid metals for electrical, optical, and sensing applications. ACS Appl. Nano Mater. *2*, 4665–4672. https://doi.org/10.1021/acsanm.9b01133.

Alsaif, M.M.Y.A., Haque, F., Alkathiri, T., Krishnamurthi, V., Walia, S., Hu, Y., Jannat, A., Mohiuddin, M., Xu, K., Khan, M.W., et al. (2021). 3D visible-light-driven plasmonic oxide frameworks deviated from liquid metal nanodroplets. Adv. Funct. Mater. *2106397*, 1–13. https://doi.org/10.1002/adfm.202106397.

Anasori, B., Lukatskaya, M.R., and Gogotsi, Y. (2017). 2D metal carbides and nitrides (MXenes) for energy storage. Nat. Rev. Mater. *2*, 16098. https://doi.org/10.1038/natrevmats.2016.98.

Apte, A., Mozaffari, K., Samghabadi, F.S., Hachtel, J.A., Chang, L., Susarla, S., Idrobo, J.C., Moore, D.C., Glavin, N.R., Litvinov, D., et al. (2020). 2D electrets of ultrathin MoO_2 with apparent piezoelectricity. Adv. Mater. *32*, 2–9. https://doi.org/10.1002/adma.202000006.

Atkin, P., Orrell-Trigg, R., Zavabeti, A., Mahmood, N., Field, M.R., Daeneke, T., Cole, I.S., and Kalantar-Zadeh, K. (2018). Evolution of 2D tin oxides on the surface of molten tin. Chem. Commun. *54*, 2102–2105. https://doi.org/10.1039/c7cc09040d.

Bayazit, M.K., Xiong, L., Jiang, C., Moniz, S.J.A., White, E., Shaffer, M.S.P., and Tang, J. (2021). Defect-free single-layer graphene by 10 s microwave solid exfoliation and its application for catalytic water splitting. ACS Appl. Mater. Inter. *24*, 28600–28609. https://doi.org/10.1021/acsami.1c03906.

Bisht, P., Kumar, A., Jensen, I.T., Ahmad, M., Belle, B.D., and Mehta, B.R. (2021). Enhanced gas sensing response for 2D α-MoO_3 layers: thickness-dependent changes in defect concentration, surface oxygen adsorption, and metal-metal oxide contact. Sensors Actuators B Chem. *341*, 129953. https://doi.org/10.1016/j.snb.2021.129953.

Cao, H., Zhou, X., Zheng, C., and Liu, Z. (2015). Two-dimensional porousmicro/nano metal oxides templated by graphene oxide. ACS Appl. Mater. Inter. *7*, 11984–11990. https://doi.org/10.1021/acsami.5b02014.

Carey, B.J., Ou, J.Z., Clark, R.M., Berean, K.J., Zavabeti, A., Chesman, A.S.R., Russo, S.P., Lau, D.W.M., Xu, Z.Q., Bao, Q., et al. (2017). Wafer-scale two-dimensional semiconductors from printed oxide skin of liquid metals. Nat. Commun. *8*, 1–10. https://doi.org/10.1038/ncomms14482.

Chen, C., Wang, M., Wu, J., Fu, H., Yang, H., Tian, Z., Tu, T., Peng, Han, Sun, Y., Xu, X., et al. (2018). Electronic structures and unusually robust bandgap in an ultrahigh-mobility layered oxide semiconductor, Bi_2O_2Se. Sci. Adv. *4*, 1–7. https://doi.org/10.1126/sciadv.aat8355.

Chen, L.Y., Gai, Y.N., Gai, X.T., Qin, J., Wang, Z.G., Cui, L.S., Guo, H., Jiang, M.Y., Zou, Q., Zhou, T., and Gai, J.G. (2021a). Interfacial synthesized covalent organic framework nanofiltration membranes for precisely ultrafast sieving. Chem. Eng. J. *430*, 133024. https://doi.org/10.1016/j.cej.2021.133024.

Chen, Z., Li, X., Yang, C., Cheng, K., Tan, T., Lv, Y., and Liu, Y. (2021b). Hybrid porous crystalline materials from metal organic frameworks and covalent organic frameworks. Adv. Sci. *8*, 1–27. https://doi.org/10.1002/advs.202101883.

Cho, Y.S., and Huh, Y.D. (2010). Controlled-synthesis and photocatalytic properties of h-In_2O_3 and c-In_2O_3. Bull. Korean Chem. Soc. *31*, 1769–1772. https://doi.org/10.5012/bkcs.2010.31.6.1769.

Daeneke, T., Atkin, P., Orrell-Trigg, R., Zavabeti, A., Ahmed, T., Walia, S., Liu, M., Tachibana, Y., Javaid, M., Greentree, A.D., et al. (2017). Wafer-scale synthesis of semiconducting SnO monolayers from interfacial oxide layers of metallic liquid tin. ACS Nano *11*, 10974–10983. https://doi.org/10.1021/acsnano.7b04856.

Datta, R.S., Syed, N., Zavabeti, A., Jannat, A., Mohiuddin, M., Rokunuzzaman, M., Yue Zhang, B., Rahman, M.A., Atkin, P., Messalea, K.A., et al. (2020). Flexible two-dimensional indium tin oxide fabricated using a liquid metal printing technique. Nat. Electron. *3*, 51–58. https://doi.org/10.1038/s41928-019-0353-8.

Di, J., Chen, C., Zhu, C., Ji, M., Xia, J., Yan, C., Hao, W., Li, S., Li, H., and Liu, Z. (2018). Bismuth vacancy mediated single unit cell Bi_2WO_6 nanosheets for boosting photocatalytic oxygen evolution. Appl. Catal. B Environ. *238*, 119–125. https://doi.org/10.1016/j.apcatb.2018.06.066.

Di, J., Zhao, X., Lian, C., Ji, M., Xia, J., Xiong, J., Zhou, W., Cao, X., She, Y., Liu, H., et al. (2019). Atomically-thin Bi_2MoO_6 nanosheets with vacancy pairs for improved photocatalytic CO_2 reduction. Nano Energy *61*, 54–59. https://doi.org/10.1016/j.nanoen.2019.04.029.

Ding, L., Wei, Y., Wang, Y., Chen, H., Caro, J., and Wang, H. (2017). A two-dimensional lamellar membrane: MXene nanosheet stacks. Angew. Chem. Int. Ed. *56*, 1825–1829. https://doi.org/10.1002/anie.201609306.

Dral, A.P., and ten Elshof, J.E. (2018). 2D metal oxide nanoflakes for sensing applications: review and perspective. Sensors Actuators B Chem. *272*, 369–392. https://doi.org/10.1016/j.snb.2018.05.157.

Du, L., Tian, Q., Zheng, X., Guo, W., Liu, W., Zhou, Y., Shi, F., and Xu, Q. (2021). Supercritical CO_2-tailored 2D oxygen-doped amorphous carbon nitride for enhanced photocatalytic activity. Energy Environ. Mater. *0*, 1–6. https://doi.org/10.1002/eem2.12209.

Dou, Y., Zhang, L., Xu, X., Sun, Z., Liao, T., and Dou, S.X. (2017). Atomically thin non-layered nanomaterials for energy storage and conversion. Chem. Soc. Rev. *46*, 7338–7373. https://doi.org/10.1039/c7cs00418d.

Fine, G.F., Cavanagh, L.M., Afonja, A., and Binions, R. (2010). Metal oxide semi-conductor gas sensors in environmental monitoring. Sensors *10*, 5469–5502. https://doi.org/10.3390/s100605469.

Fujito, H., Kunioku, H., Kato, D., Suzuki, H., Higashi, M., Kageyama, H., and Abe, R. (2016). Layered perovskite oxychloride Bi_4NbO_8Cl: a stable visible light responsive photocatalyst for water splitting. J. Am. Chem. Soc. *138*, 2082–2085. https://doi.org/10.1021/jacs.5b11191.

Fujihara, S., Hosono, E., and Kimura, T. (2004). Fabrication of porous metal oxide semiconductor films by a self-template method using layered hydroxide metal acetates. J. Sol-Gel Sci. Technol. *31*, 165–168. https://doi.org/10.1023/B:JSST.0000047980.69279.9b.

Gou, G., Zhao, M., Shi, J., Harada, J.K., and Rondinelli, J.M. (2020). Anion ordered and ferroelectric ruddlesden-popper oxynitride $Ca_3Nb_2N_2O_5$ for visible-light-active photocatalysis. Chem. Mater. *32*, 2815–2823. https://doi.org/10.1021/acs.chemmater.9b04429.

Gao, Q., Cui, Y., Zhang, H., Wang, S., Liu, B., and Liu, C. (2021). Construction of Z-scheme 1D CdS nanorods/2D ultrathin CeO_2 nanosheets toward enhanced photodegradation and hydrogen evolution. Sep. Purif. Technol. *274*, 119116. https://doi.org/10.1016/j.seppur.2021.119116.

Ge, T., Wei, Z., Zheng, X., and Xu, Q. (2021). CO_2-assisted synthesis of 2D amorphous MoO_{3-x} nanosheets: From top-down to bottom-up. J. Phys. Chem. Lett. *12*, 1554–1559. https://doi.org/10.1021/acs.jpclett.1c00012.

Ge, T., Wei, Z., Zheng, X., Yan, P., and Xu, Q. (2021b). Atomic rearrangement and amorphization induced by carbon dioxide in two-dimensional MoO_{3-x} nanomaterials. J. Phys. Chem. Lett. *12*, 6543–6550. https://doi.org/10.1021/acs.jpclett.1c01703.

Ghasemian, M.B., Mayyas, M., Idrus-Saidi, S.A., Jamal, M.A., Yang, J., Mofarah, S.S., Adabifiroozjaei, E., Tang, J., Syed, N., O'Mullane, A.P., et al. (2019). Self-limiting galvanic growth of MnO_2 monolayers on a liquid metal-applied to photocatalysis. Adv. Funct. Mater. *29*, 1–12. https://doi.org/10.1002/adfm.201901649.

Ghasemian, M.B., Zavabeti, A., Abbasi, R., Kumar, P.V., Syed, N., Yao, Y., Tang, J., Wang, Y., Elbourne, A., Han, J., et al. (2020). Ultra-thin lead oxide piezoelectric layers for reduced environmental contamination using a liquid metal-based process. J. Mater. Chem. A. *8*, 19434–19443. https://doi.org/10.1039/d0ta06379g.

Goff, A., Aukarasereenont, P., Nguyen, C.K., Grant, R., Syed, N., Zavabeti, A., Elbourne, A., and Daeneke, T. (2021). An exploration into two-dimensional metal oxides, and other 2D

materials, synthesisedvialiquid metal printing and transfer techniques. Dalt. Trans. *50*, 7513–7526. https://doi.org/10.1039/d0dt04364h.

Gu, J., Zhang, C., Du, Z., and Yang, S. (2019). Rapid and low-temperature salt-templated production of 2D metal oxide/oxychloride/hydroxide. Small *15*, 1904587. https://doi.org/10.1002/smll.201904587.

Guo, C., Yan, P., Zhu, C., Wei, C., Liu, W., Wu, W., Wang, X., Zheng, L., Wang, J., Du, Y., et al. (2019). Amorphous MoO_{3-x} nanosheets prepared by the reduction of crystalline MoO_3 by Mo metal for LSPR and photothermal conversion. Chem. Commun. *55*, 12527–12530. https://doi.org/10.1039/c9cc06704c.

Guo, Y., Kang, L., Song, P., Zeng, Q., Tang, B., Yang, J., Wu, Y., Tian, D., Xu, M., Zhao, W., et al. (2021). MoO_3-MoS_2 vertical heterostructures synthesized via one-step CVD process for optoelectronics. 2D Mater. *8*, 035036. https://doi.org/10.1088/2053-1583/abfede.

Hong, C., Tao, Y., Nie, A., Zhang, M., Wang, N., Li, R., Huang, J., Huang, Y., Ren, X., Cheng, Y., and Liu, X. (2020). Inclined ultrathin Bi_2O_2Se films: a building block for functional van der Waals heterostructures. ACS Nano. *14*, 16803–16812. https://doi.org/10.1021/acsnano.0c05300.

Hanlon, D., Backes, C., Higgins, T.M., Hughes, M., O'Neill, A., King, P., McEvoy, N., Duesberg, G.S., Mendoza Sanchez, B., Pettersson, H., et al. (2014). Production of molybdenum trioxide nanosheets by liquid exfoliation and their application in high-performance supercapacitors. Chem. Mater. *26*, 1751–1763. https://doi.org/10.1021/cm500271u.

Haque, F., Daeneke, T., Kalantar-zadeh, K., and Ou, J.Z. (2018). Two-dimensional transition metal oxide and chalcogenide-based photocatalysts. Nanomicro Lett. *10*, 23. https://doi.org/10.1007/s40820-017-0176-y.

Haque, F., Zavabeti, A., Zhang, B.Y., Datta, R.S., Yin, Y., Yi, Z., Wang, Y., Mahmood, N., Pillai, N., Syed, N., et al. (2019). Ordered intracrystalline pores in planar molybdenum oxide for enhanced alkaline hydrogen evolution. J. Mater. Chem. A. *7*, 257–268. https://doi.org/10.1039/c8ta08330d.

Hoshyargar, F., Crawford, J., and O'Mullane, A.P. (2017). Galvanic replacement of the liquid metal galinstan. J. Am. Chem. Soc. *139*, 1464–1471. https://doi.org/10.1021/jacs.6b05957.

Hou, C., Zhang, M., Zhang, L., Tang, Y., Wang, H., and Chi, Q. (2017). Reagent-free electrophoretic synthesis of few-atom-thick metal oxide nanosheets. Chem. Mater. *29*, 1439–1446. https://doi.org/10.1021/acs.chemmater.7b00188.

Hu, Z., Yuan, T., Li, H., Qiu, Y., Zhou, W., Zhang, J., Zhao, Y., and Hu, S. (2021). Two-dimensional oxide derived from high-temperature liquid metals via bubble templating. Nano Res. *12*, 1–7. https://doi.org/10.1007/s12274-021-3430-z.

Huang, Y., Sutter, E., Shi, N.N., Zheng, J., Yang, T., Englund, D., Gao, H.J., and Sutter, P. (2015). Reliable exfoliation of large-area high-quality flakes of graphene and other two-dimensional materials. ACS Nano *9*, 10612–10620. https://doi.org/10.1021/acsnano.5b04258.

Huang, Z., Zhou, A., Wu, J., Chen, Y., Lan, X., Bai, H., and Li, L. (2016). Bottom-up preparation of ultrathin 2D aluminum oxide nanosheets by duplicating graphene oxide. Adv. Mater. *28*, 1703–1708. https://doi.org/10.1002/adma.201504484.

Huo, C., Yan, Z., Song, X., and Zeng, H. (2015). 2D materials via liquid exfoliation: a review on fabrication and applications. Sci. Bull. *60*, 1994–2008. https://doi.org/10.1007/s11434-015-0936-3.

Jannat, A., Syed, N., Xu, K., Rahman, M.A., Talukder, M.M.M., Messalea, K.A., Mohiuddin, M., Datta, R.S., Khan, M.W., Alkathiri, T., et al. (2021). Printable single-unit-cell-thick transparent zinc-doped indium oxides with efficient electron transport properties. ACS Nano *15*, 4045–4053. https://doi.org/10.1021/acsnano.0c06791.

Jannat, A., Yao, Q., Zavabeti, A., Syed, N., Zhang, B.Y., Ahmed, T., Kuriakose, S., Mohiuddin, M., Pillai, N., Haque, F., et al. (2020). Ordered-vacancy-enabled indium sulphide printed in wafer-scale with enhanced electron mobility. Mater. Horizons. *7*, 827–834. https://doi.org/10.1039/c9mh01365b.

Jia, B., Yang, J., Hao, R., Li, L., and Guo, L. (2020). Confined synthesis of ultrathin amorphous metal-oxide nanosheets. ACS Mater. Lett. *2*, 610–615. https://doi.org/10.1021/acsmaterialslett.0c00114.

Kato, D., Hongo, K., Maezono, R., Higashi, M., Kunioku, H., Yabuuchi, M., Suzuki, H., Okajima, H., Zhong, C., Nakano, K., et al. (2017). Valence band engineering of layered bismuth oxyhalides toward stable visible-light water splitting: madelung site potential analysis. J. Am. Chem. Soc. *139*, 18725–18731. https://doi.org/10.1021/jacs.7b11497.

Kalantar-Zadeh, K., Ou, J.Z., Daeneke, T., Mitchell, A., Sasaki, T., and Fuhrer, M.S. (2016). Two dimensional and layered transition metal oxides. Appl. Mater. Today *5*, 73–89. https://doi.org/10.1016/j.apmt.2016.09.012.

Kalantar-Zadeh, K., Tang, J., Daeneke, T., O'Mullane, A.P., Stewart, L.A., Liu, J., Majidi, C., Ruoff, R.S., Weiss, P.S., and Dickey, M.D. (2019). Emergence of liquid metals in nanotechnology. ACS Nano *13*, 7388–7395. https://doi.org/10.1021/acsnano.9b04843.

Khan, H., Zavabeti, A., Wang, Y., Harrison, C.J., Carey, B.J., Mohiuddin, M., Chrimes, A.F., De Castro, I.A., Zhang, B.Y., Sabri, Y.M., et al. (2017). Quasi physisorptive two dimensional tungsten oxide nanosheets with extraordinary sensitivity and selectivity to NO_2. Nanoscale *9*, 19162–19175. https://doi.org/10.1039/c7nr05403c.

Khan, M.W., Zhang, B.Y., Xu, K., Mohiuddin, M., Jannat, A., Haque, F., Alkathiri, T., Pillai, N., Wang, Y., Reza, S.Z., et al. (2021). Plasmonic metal-organic framework nanocomposites enabled by degenerately doped molybdenum oxides. J. Colloid Interf. Sci. *588*, 305–314. https://doi.org/10.1016/j.jcis.2020.12.070.

Kim, H.U., Son, J., Kulkarni, A., Ahn, C., Kim, K.S., Shin, D., Yeom, G.Y., and Kim, T. (2017). Highly uniform wafer-scale synthesis of α-MoO_3 by plasma enhanced chemical vapor deposition. Nanotechnology *28*, 175601. https://doi.org/10.1088/1361-6528/aa67d1.

Kim, J., Kwon, S., Cho, D.H., Kang, B., Kwon, H., Kim, Y., Park, S.O., Jung, G.Y., Shin, E., Kim, W.G., et al. (2015). Direct exfoliation and dispersion of two-dimensional materials in pure water via temperature control. Nat. Commun. *6*, 8294. https://doi.org/10.1038/ncomms9294.

Kumbhakar, P., Chowde Gowda, C., Mahapatra, P.L., Mukherjee, M., Malviya, K.D., Chaker, M., Chandra, A., Lahiri, B., Ajayan, P.M., Jariwala, D., et al. (2021). Emerging 2D metal oxides and their applications. Mater. Today *45*, 142–168. https://doi.org/10.1016/j.mattod.2020.11.023.

Lan, K., Liu, Yao, Zhang, W., Liu, Yong, Elzatahry, A., Wang, R., Xia, Y., Al-Dhayan, D., Zheng, N., and Zhao, D. (2018). Uniform ordered two-dimensional mesoporous TiO_2 nanosheets from hydrothermal-induced solvent-confined monomicelle assembly. J. Am. Chem. Soc. *140*, 4135–4143. https://doi.org/10.1021/jacs.8b00909.

Lee, W.J., and Sung, Y.M. (2012). Synthesis of anatase nanosheets with exposed (001) facets via chemical vapor deposition. Cryst. Growth Des. *12*, 5792–5795. https://doi.org/10.1021/cg301317j.

Lei, F., Sun, Y., Liu, K., Gao, S., Liang, L., Pan, B., and Xie, Y. (2014). Oxygen vacancies confined in ultrathin indium oxide porous sheets for promoted visible-light water splitting. J. Am. Chem. Soc. *136*, 6826–6829. https://doi.org/10.1021/ja501866r.

Lertanantawong, B., Lertsathitphong, P., and O'Mullane, A.P. (2018). Chemical reactivity of Ga-based liquid metals with redox active species and its influence on electrochemical processes. Electrochem. Commun. *93*, 15–19. https://doi.org/10.1016/j.elecom.2018.05.026.

Li, Z., Ru, L., Bai, C., Zhang, N., and Wang, H. (2013). Effect of $CaTiO_3$ crystal structure and cathodic morphological structure on the electrolysis. Asian J. Chem. *25*, 1814–1818. https://doi.org/10.14233/ajchem.2013.13162.

Li, H., Xu, Q., Wang, X., and Liu, W. (2018). Ultrasensitive surface-enhanced Raman spectroscopy detection based on amorphous molybdenum oxide quantum dots. Small *14*, 1–9. https://doi.org/10.1002/smll.201801523.

Li, J., Zhang, X., Yang, B., Zhang, C., Xu, T., Chen, L., Yang, L., Jin, X., and Liu, B. (2021a). Template approach to large-area non-layered Ga-group two-dimensional crystals from printed skin of liquid gallium. Chem. Mater. *33*, 4568–4577. https://doi.org/10.1021/acs.chemmater.1c00999.

Li, L., Lu, F., Xiong, W., Ding, Y., Lu, Y., Xiao, Y., Tong, X., Wang, Y., Jia, S., Wang, J., et al. (2021b). General synthesis of 2D rare-earth oxides single crystals with tailorable facet. Natl. Sci. Rev. https://doi.org/10.1093/nsr/nwab153.

Li, Z., Yao, Z., Haidry, A.A., Luan, Y., Chen, Y., Zhang, B.Y., Xu, K., Deng, R., Duc Hoa, N., Zhou, J., and Ou, J.Z. (2021c). Recent advances of atomically thin 2D heterostructures in sensing applications. Nano Today *40*, 101287. https://doi.org/10.1016/j.nantod.2021.101287.

Lin, Z., Wang, C., and Chai, Y. (2020). Emerging group-VI elemental 2D materials: Preparations, properties, and device applications. Small *16*, 1–16. https://doi.org/10.1002/smll.202003319.

Lei, Z., Lee, J.M., Singh, G., Sathish, C.I., Chu, X., Al-Muhtaseb, A.H., Vinu, A., and Yi, J. (2021). Recent advances of layered-transition metal oxides for energy-related applications. Energy Storage Mater. *36*, 514–550. https://doi.org/10.1016/j.ensm.2021.01.004.

Liu, S., Xie, L., Qian, H., Liu, G., Zhong, H., and Zeng, H. (2019). Facile preparation of novel and active 2D nanosheets from non-layered and traditionally non-exfoliable earth-abundant materials. J. Mater. Chem. A. *7*, 15411–15419. https://doi.org/10.1039/c9ta04442f.

Liu, W., and Xu, Q. (2018). CO_2-assisted conversion of crystal two-dimensional molybdenum oxide to amorphism with plasmon resonances. Chem. Eur. J. *24*, 13693–13700. https://doi.org/10.1002/chem.201801055.

Liu, W., Xu, Q., Cui, W., Zhu, C., and Qi, Y. (2017). CO_2-assisted fabrication of two-dimensional amorphous molybdenum oxide nanosheets for enhanced plasmon resonances. Angew. Chem. Int. Ed. *56*, 1600–1604. https://doi.org/10.1002/anie.201610708.

Liu, W., Xu, Q., and Zhou, Y. (2020). CO_2-assisted fabrication of two-dimensional amorphous transition metal oxides. Dalt. Trans. *49*, 2048–2052. https://doi.org/10.1039/c9dt04651h.

Liu, Y., Che, R., Chen, G., Fan, J., Sun, Z., Wu, Z., Wang, M., Li, B., Wei, J., Wei, Y., et al. (2015). Radially oriented mesoporous TiO_2 microspheres with single-crystal-like anatase walls for high-efficiency optoelectronic devices. Sci. Adv. *1*, 1–8. https://doi.org/10.1126/sciadv.1500166.

Luo, J., Chen, H., Wang, J., Xia, F., and Huang, X. (2020). Direct growth of 2D MoO_2 single crystal on SiO_2/Si substrate by atmospheric pressure chemical vapor deposition. Mater. Chem. Phys. *251*, 123166. https://doi.org/10.1016/j.matchemphys.2020.123166.

Luo, P., Wang, F., Qu, J., Liu, K., Hu, X., Liu, K., and Zhai, T. (2021). Self-driven WSe_2/Bi_2O_2Se van der Waals heterostructure photodetectors with high light on/off ratio and fast response. Adv. Funct. Mater. *31*, 1–9. https://doi.org/10.1002/adfm.202008351.

Lv, H., Wu, C., Tang, J., Du, H., Qin, F., Peng, H., and Yan, M. (2021). Two-dimensional SnO/SnO_2 heterojunctions for electromagnetic wave absorption. Chem. Eng. J. *411*, 128445. https://doi.org/10.1016/j.cej.2021.128445.

Lv, L., Yang, Z., Chen, K., Wang, C., and Xiong, Y. (2019). 2D layered double hydroxides for oxygen evolution reaction: from fundamental design to application. Adv. Energy Mater. *9*, 1–29. https://doi.org/10.1002/aenm.201803358.

Lv, R., Robinson, J.A., Schaak, R.E., Sun, D., Sun, Y., Mallouk, T.E., and Terrones, M. (2015). Transition metal dichalcogenides and beyond: synthesis, properties, and applications of single- and few-layer nanosheets. Acc. Chem. Res. *48*, 56–64. https://doi.org/10.1021/ar5002846.

Mannix, A.J., Zhang, Z., Guisinger, N.P., Yakobson, B.I., and Hersam, M.C. (2018). Borophene as a prototype for synthetic 2D materials development. Nat. Nanotechnol. *13*, 444–450. https://doi.org/10.1038/s41565-018-0157-4.

Mei, J., Liao, T., Kou, L., and Sun, Z. (2017). Two-dimensional metal oxide nanomaterials for next-generation rechargeable batteries. Adv. Mater. *29*, 1–25. https://doi.org/10.1002/adma.201700176.

Mahmood, N., De Castro, I.A., Pramoda, K., Khoshmanesh, K., Bhargava, S.K., and Kalantar-Zadeh, K. (2019). Atomically thin two-dimensional metal oxide nanosheets and their heterostructures for energy storage. Energy Storage Mater. *16*, 455–480. https://doi.org/10.1016/j.ensm.2018.10.013.

Mahmood, N., Khan, H., Tran, K., Kuppe, P., Zavabeti, A., Atkin, P., Ghasemian, M.B., Yang, J., Xu, C., Tawfik, S.A., et al. (2021). Maximum piezoelectricity in a few unit-cell thick planar ZnO-a liquid metal-based synthesis approach. Mater. Today *44*, 69–77. https://doi.org/10.1016/j.mattod.2020.11.016.

Manzeli, S., Ovchinnikov, D., Pasquier, D., Yazyev, O.V., and Kis, A. (2017). 2D transition metal dichalcogenides. Nat. Rev. Mater. *2*, 17033. https://doi.org/10.1038/natrevmats.2017.33.

Ma, S., Cai, M., Cheng, T., Ding, X., Shi, X., Alsaedi, A., Hayat, T., Ding, Y., Tan, Z., and Dai, S. (2018). Two-dimensional organic-inorganic hybrid perovskite: from material properties to device applications. Sci. China Mater. *61*, 1257–1277. https://doi.org/10.1007/s40843-018-9294-5.

Messalea, K.A., Carey, B.J., Jannat, A., Syed, N., Mohiuddin, M., Zhang, B.Y., Zavabeti, A., Ahmed, T., Mahmood, N., Della Gaspera, E., et al. (2018). Bi_2O_3 monolayers from elemental liquid bismuth. Nanoscale *10*, 15615–15623. https://doi.org/10.1039/c8nr03788d.

Messalea, K.A., Zavabeti, A., Mohiuddin, M., Syed, N., Jannat, A., Atkin, P., Ahmed, T., Walia, S., McConville, C.F., Kalantar-Zadeh, K., et al. (2020). Two-step synthesis of large-area 2D Bi_2S_3 nanosheets featuring high in-plane anisotropy. Adv. Mater. Inter. *7*, 1–8. https://doi.org/10.1002/admi.202001131.

Mohiuddin, M., Zavabeti, A., Haque, F., Mahmood, A., Datta, R.S., Syed, N., Khan, M.W., Jannat, A., Messalea, K., Zhang, B.Y., et al. (2020). Synthesis of two-dimensional hematite and iron phosphide for hydrogen evolution. J. Mater. Chem. A. *8*, 2789–2797. https://doi.org/10.1039/c9ta11945k.

Matsumoto, Y., Nambu, Y., Honda, T., Ikeda, K., Otomo, T., and Kageyama, H. (2020). High-pressure synthesis of $Ba_2CoO_2Ag_2Te_2$ with extended CoO_2 planes. Inorg. Chem. *59*, 8121–8126. https://doi.org/10.1021/acs.inorgchem.0c00429.

Nagyné-Kovács, T., Studnicka, L., Lukács, I.E., László, K., Pasierb, P., Szilágyi, I.M., and Pokol, G. (2020). Hydrothermal synthesis and gas sensing of monoclinic MoO_3 nanosheets. Nanomaterials *10*, 2–13. https://doi.org/10.3390/nano10050891.

Nguyen, C., Syed, N., Low, M.X., Zavabeti, A., Jannat, A., Murdoch, B.J., Della Gaspera, E., Orrell-Trigg, R., Walia, S., Elbourne, A.J., et al. (2021). Ultrathin oxysulfide semiconductors from liquid metal: a wet chemical approach. J. Mater. Chem. C *9*, 11815. https://doi.org/10.1039/d1tc01937f.

Nicolosi, V., Chhowalla, M., Kanatzidis, M.G., Strano, M.S., and Coleman, J.N. (2013). Liquid exfoliation of layered materials. Science *340*, 72–75. https://doi.org/10.1126/science.1226419.

Novoselov, K.S., Geim, A.K., Morozov, S.V., Jiang, D., Katsnelson, M.I., Grigorieva, I.V., Dubonos, S.V., and Firsov, A.A. (2004). Electric field effect in atomically thin carbon films. Science *306*, 5696. https://doi.org/10.1126/science.1102896.

Ou, J., Yan, J., Xu, T., Jiang, Z., Tan, H., He, S., Hu, B., and Yu, G. (2021). Fabrication of nickel-iron layered double hydroxides using nickel plating wastewater via electrocoagulation, and its use for efficient dye removal. J. Mol. Liq. *335*, 116246. https://doi.org/10.1016/j.molliq.2021.116246.

Oshima, T., Ichibha, T., Oqmhula, K., Hibino, K., Mogi, H., Yamashita, S., Fujii, K., Miseki, Y., Hongo, K., Lu, D., et al. (2020). Two-dimensional perovskite oxynitride $K_2LaTa_2O_6N$ with an H^+/K^+ exchangeability in aqueous solution forming a stable photocatalyst for visible-light H_2 evolution. Angew. Chem. Int. Ed. Engl. *59*, 9736–9743. https://doi.org/10.1002/anie.202002534.

Oshima, T., Ichibha, T., Qin, K.S., Muraoka, K., Vequizo, J.J.M., Hibino, K., Kuriki, R., Yamashita, S., Hongo, K., Uchiyama, T., et al. (2018). Undoped layered perovskite oxynitride $Li_2LaTa_2O_6N$ for photocatalytic CO_2 reduction with visible light. Angew. Chem. Int. Ed. Engl. *57*, 8154–8158. https://doi.org/10.1002/anie.201803931.

Pi, L., Li, L., Liu, K., Zhang, Q., Li, H., and Zhai, T. (2019). Recent progress on 2D noble-transition-metal dichalcogenides. Adv. Funct. Mater. *29*, 1–22. https://doi.org/10.1002/adfm.201904932.

Puthirath Balan, A., Radhakrishnan, S., Kumar, R., Neupane, R., Sinha, S.K., Deng, L., De Los Reyes, C.A., Apte, A., Rao, B.M., Paulose, M., et al. (2018a). A non-van der Waals two-dimensional material from natural titanium mineral ore ilmenite. Chem. Mater. *30*, 5923–5931. https://doi.org/10.1021/acs.chemmater.8b01935.

Puthirath Balan, A., Radhakrishnan, S., Woellner, C.F., Sinha, S.K., Deng, L., Reyes, C.D.L., Rao, B.M., Paulose, M., Neupane, R., Apte, A., et al. (2018b). Exfoliation of a non-van der Waals material from iron ore hematite. Nat. Nanotechnol. *13*, 602–609. https://doi.org/10.1038/s41565-018-0134-y.

Qin, B., Ma, H., Hossain, M., Zhong, M., Xia, Q., Li, B., and Duan, X. (2020). Substrates in the synthesis of two-dimensional materials via chemical vapor deposition. Chem. Mater. *32*, 10321–10347. https://doi.org/10.1021/acs.chemmater.0c03549.

Ren, B., Wang, Y., and Ou, J.Z. (2020). Engineering two-dimensional metal oxides: via surface functionalization for biological applications. J. Mater. Chem. B *8*, 1108–1127. https://doi.org/10.1039/c9tb02423a.

Ren, G., Zhang, B.Y., Yao, Q., Zavabeti, A., Huertas, C.S., Brkljača, R., Khan, M.W., Nili, H., Datta, R.S., Khan, H., et al. (2019). An ultrasensitive silicon photonic ion sensor enabled by 2D plasmonic molybdenum oxide. Small *15*, 1–10. https://doi.org/10.1002/smll.201805251.

Ren, Y., and Xu, Q. (2018). Building close ties between CO_2 and functional two-dimensional nanomaterials with green chemistry strategy.

Energy Environ. Mater. *1*, 46–60. https://doi.org/10.1002/eem2.12005.

Rui, X., Lu, Z., Yu, H., Yang, D., Hng, H.H., Lim, T.M., and Yan, Q. (2013). Ultrathin V_2O_5 nanosheet cathodes: Realizing ultrafast reversible lithium storage. Nanoscale *5*, 556–560. https://doi.org/10.1039/c2nr33422d.

Saeed, M., Uddin, W., Saleemi, A.S., Hafeez, M., Kamil, M., Mir, I.A., Sunila, Ullah, R., Rehman, S.U., and Ling, Z. (2020). Optoelectronic properties of MoS_2-ReS_2 and ReS_2-MoS_2 heterostructures. Phys. B Condens. Matter. *577*, 411809. https://doi.org/10.1016/j.physb.2019.411809.

Sahu, K., Choudhary, S., Singh, J., Kuriakose, S., Singhal, R., and Mohapatra, S. (2018). Facile wet chemical synthesis of ZnO nanosheets: effects of counter ions on the morphological, structural, optical and photocatalytic properties. Ceram. Int. *44*, 23094–23101. https://doi.org/10.1016/j.ceramint.2018.09.116.

Sethulakshmi, N., Mishra, A., Ajayan, P.M., Kawazoe, Y., Roy, A.K., Singh, A.K., and Tiwary, C.S. (2019). Magnetism in two-dimensional materials beyond graphene. Mater. Today *27*, 107–122. https://doi.org/10.1016/j.mattod.2019.03.015.

Shangguan, C., Dong, M., Ren, G., Lu, L., Zhang, B.Y., Ma, Q., Xu, K., Hu, Y., Alkathiri, T., You, R., et al. (2021). Angstrom-scale-porous plasmonic molybdenum oxide for ultrasensitive optical chemical sensing. Sensors Actuators B Chem. *349*, 130740. https://doi.org/10.1016/j.snb.2021.130740.

Si, J., Yu, J., Shen, Y., Zeng, M., and Fu, L. (2021). Elemental 2D materials: Progress and perspectives toward unconventional structures. Small Struct. *2*, 2000101. https://doi.org/10.1002/sstr.202000101.

Shi, J., Zhang, J., Yang, L., Qu, M., Qi, D.C., and Zhang, K.H.L. (2021). Wide bandgap oxide semiconductors: from materials physics to optoelectronic devices. Adv. Mater. 1–30. https://doi.org/10.1002/adma.202006230.

Siddique, S., Chowde Gowda, C., Demiss, S., Tromer, R., Paul, S., Sadasivuni, K.K., Olu, E.F., Chandra, A., Kochat, V., Galvão, D.S., et al. (2021). Emerging two-dimensional tellurides. Mater. Today. https://doi.org/10.1016/j.mattod.2021.08.008.

Song, C., Zhao, J., Li, H., Luo, S., Tang, Y., and Wang, D. (2017). Design, controlled synthesis, and properties of 2D CeO_2/NiO heterostructure assemblies. CrystEngComm *19*, 7339–7346. https://doi.org/10.1039/c7ce01769c.

Sricharan, M., Gupta, B., Moolayadukkam, S., and Matte, H.S.S.R. (2020). Exfoliation in a low boiling point solvent and electrochemical applications of MoO_3. Beilstein J. Nanotechnol. *11*, 662–670. https://doi.org/10.3762/bjnano.11.52.

Sun, Y., Liu, Q., Gao, S., Cheng, H., Lei, F., Sun, Z., Jiang, Y., Su, H., Wei, S., and Xie, Y. (2013). Pits confined in ultrathin cerium (IV) oxide for studying catalytic centers in carbon monoxide oxidation. Nat. Commun. *4*, 1–8. https://doi.org/10.1038/ncomms3899.

Sun, Z., Liao, T., Dou, Y., Hwang, S.M., Park, M.S., Jiang, L., Kim, J.H., and Dou, S.X. (2014). Generalized self-assembly of scalable two-dimensional transition metal oxide nanosheets. Nat. Commun. *5*, 3813. https://doi.org/10.1038/ncomms4813.

Sun, Z., Liao, T., and Kou, L. (2017). Strategies for designing metal oxide nanostructures. Sci. China Mater. *60*, 1–24. https://doi.org/10.1007/s40843-016-5117-0.

Syed, N., Zavabeti, A., Messalea, K.A., Della Gaspera, E., Elbourne, A., Jannat, A., Mohiuddin, M., Zhang, B.Y., Zheng, G., Wang, L., et al. (2019). Wafer-sized ultrathin gallium and indium nitride nanosheets through the ammonolysis of liquid metal derived oxides. J. Am. Chem. Soc. *141*, 104–108. https://doi.org/10.1021/jacs.8b11483.

Syed, N., Zavabeti, A., Mohiuddin, M., Zhang, B., Wang, Y., Datta, R.S., Atkin, P., Carey, B.J., Tan, C., van Embden, J., et al. (2017). Sonication-assisted synthesis of gallium oxide suspensions featuring trap state absorption: test of photochemistry. Adv. Funct. Mater. *27*, 1–10. https://doi.org/10.1002/adfm.201702295.

Syed, N., Zavabeti, A., Ou, J.Z., Mohiuddin, M., Pillai, N., Carey, B.J., Zhang, B.Y., Datta, R.S., Jannat, A., Haque, F., et al. (2018). Printing two-dimensional gallium phosphate out of liquid metal. Nat. Commun. *9*, 1–10. https://doi.org/10.1038/s41467-018-06124-1.

Takenaka, S., Miyake, S., Uwai, S., Matsune, H., and Kishida, M. (2015). Preparation of metal oxide nanofilms using graphene oxide as a template. J. Phys. Chem. C *119*, 12445–12454. https://doi.org/10.1021/acs.jpcc.5b02447.

Tan, C., Cao, X., Wu, X.J., He, Q., Yang, J., Zhang, X., Chen, J., Zhao, W., Han, S., Nam, G.H., et al. (2017). Recent advances in ultrathin two-dimensional nanomaterials. Chem. Rev. *117*, 6225–6331. https://doi.org/10.1021/acs.chemrev.6b00558.

Tao, J., Luttrell, T., and Batzill, M. (2011). A two-dimensional phase of TiO_2 with a reduced bandgap. Nat. Chem. *3*, 296–300. https://doi.org/10.1038/nchem.1006.

Tong, X., Liu, K., Zeng, M., and Fu, L. (2019). Vapor-phase growth of high-quality wafer-scale two-dimensional materials. InfoMat *1*, 460–478. https://doi.org/10.1002/inf2.12038.

Wang, J., and Liu, C.J. (2015). Preparation of 2D WO_3 nanomaterials with enhanced catalytic activities: Current status and perspective. Chem. Bio. Eng. Rev. *2*, 335–350. https://doi.org/10.1002/cben.201500014.

Wang, B., Di, J., Zhang, P., Xia, J., Dai, S., and Li, H. (2017a). Ionic liquid-induced strategy for porous perovskite-like $PbBiO_2Br$ photocatalysts with enhanced photocatalytic activity and mechanism insight. Appl. Catal. B Environ. *206*, 127–135. https://doi.org/10.1016/j.apcatb.2016.12.049.

Wang, F., Wang, Z., Shifa, T.A., Wen, Y., Wang, F., Zhan, X., Wang, Q., Xu, K., Huang, Y., Yin, L., et al. (2017b). Two-dimensional non-layered materials: Synthesis, properties and applications. Adv. Funct. Mater. *27*, 1603254. https://doi.org/10.1002/adfm.201603254.

Wang, Q., Nakabayashi, M., Hisatomi, T., Sun, S., Akiyama, S., Wang, Z., Pan, Z., Xiao, X., Watanabe, T., Yamada, T., et al. (2019). Oxysulfide photocatalyst for visible-light-driven overall water splitting. Nat. Mater. *18*, 827–832. https://doi.org/10.1038/s41563-019-0399-z.

Wang, P.F., Hu, Q., Lv, B., Zhu, J.L., Ma, W., Dong, Z., Wei, J., and Sun, J.L. (2020). Facile fabrication of eutectic gallium-indium alloy nanostructure and application in photodetection. Nanotechnology *31*, 145703. https://doi.org/10.1088/1361-6528/ab61d0.

Wang, F., Yang, S., Wu, J., Hu, X., Li, Y., Li, H., Liu, X., Luo, J., and Zhai, T. (2021a). Emerging two-dimensional bismuth oxychalcogenides for electronics and optoelectronics. Info. Mat. *3*, 1251–1271. https://doi.org/10.1002/inf2.12215.

Wang, Y., Liu, L., Ma, T., Zhang, Y., and Huang, H. (2021b). 2D graphitic carbon nitride for energy conversion and storage. Adv. Funct. Mater. *31*, 1–36. https://doi.org/10.1002/adfm.202102540.

Wang, Y., Mayyas, M., Yang, J., Ghasemian, M.B., Tang, J., Mousavi, M., Han, J., Ahmed, M., Baharfar, M., Mao, G., et al. (2021c). Liquid-metal-assisted deposition and patterning of molybdenum dioxide at low temperature. ACS Appl. Mater. Inter. *13*, 53181–53193. https://doi.org/10.1021/acsami.1c15367.

Wang, Y., Mayyas, M., Yang, J., Tang, J., Ghasemian, M.B., Han, J., Elbourne, A., Daeneke, T., Kaner, R.B., and Kalantar-Zadeh, K. (2021d). Self-deposition of 2D molybdenum sulfides on liquid metals. Adv. Funct. Mater. *31*, 1–9. https://doi.org/10.1002/adfm.202005866.

Wang, Y., Ren, B., Zhen Ou, J., Xu, K., Yang, C., Li, Y., and Zhang, H. (2021e). Engineering two-dimensional metal oxides and chalcogenides for enhanced electro- and photocatalysis. Sci. Bull. *66*, 1228–1252. https://doi.org/10.1016/j.scib.2021.02.007.

Wu, J., Yuan, H., Meng, M., Chen, C., Sun, Y., Chen, Z., Dang, W., Tan, C., Liu, Y., Yin, J., et al. (2017). High electron mobility and quantum oscillations in non-encapsulated ultrathin semiconducting Bi_2O_2Se. Nat. Nanotechnol. *12*, 530–534. https://doi.org/10.1038/nnano.2017.43.

Wei, Q., Li, R., Lin, C., Han, A., Nie, A., Li, Y., Li, L.J., Cheng, Y., and Huang, W. (2019). Quasi-two-dimensional Se-terminated bismuth oxychalcogenide (Bi_2O_2Se). ACS Nano *13*, 13439–13444. https://doi.org/10.1021/acsnano.9b07000.

Wei, S., and Xu, X. (2018). Boosting photocatalytic water oxidation reactions over strontium tantalum oxynitride by structural laminations. Appl. Catal. B Environ. *228*, 10–18. https://doi.org/10.1016/j.apcatb.2018.01.071.

Wei, Z., Hai, Z., Akbari, M.K., Qi, D., Xing, K., Zhao, Q., Verpoort, F., Hu, J., Hyde, L., and Zhuiykov, S. (2018). Atomic layer deposition-developed two-dimensional α-MoO_3 windows excellent hydrogen peroxide electrochemical sensing capabilities. Sensors Actuators B Chem. *262*, 334–344. https://doi.org/10.1016/j.snb.2018.01.243.

Xiao, X., Song, H., Lin, S., Zhou, Y., Zhan, X., Hu, Z., Zhang, Q., Sun, J., Yang, B., Li, T., et al. (2016). Scalable salt-templated synthesis of two-dimensional transition metal oxides. Nat.

Commun. *7*, 1–8. https://doi.org/10.1038/ncomms11296.

Xu, C., Qiu, P., Chen, H., Jiang, F., and Wang, X. (2019). Fabrication of two-dimensional indium oxide nanosheets with graphitic carbon nitride nanosheets as sacrificial templates. Mater. Lett. *242*, 24–27. https://doi.org/10.1016/j.matlet.2019.01.101.

Xu, K., Zhang, B.Y., Mohiuddin, M., Ha, N., Wen, X., Zhou, C., Li, Y., Ren, G., Zhang, H., Zavabeti, A., and Ou, J.Z. (2021). Free-standing ultrathin janus indium oxysulfide for ultrasensitive visible-light-driven optoelectronic chemical sensing. Nano Today *37*, 101096. https://doi.org/10.1016/j.nantod.2021.101096.

Xue, L., Li, S., Shen, T., Ni, M., Qiu, C., Sun, S., Geng, H., Zhu, X., and Xia, H. (2020). Two-dimensional metal (oxy)hydroxide and oxide ultrathin nanosheets via liquid phase epitaxy. Energy Storage Mater *32*, 272–280. https://doi.org/10.1016/j.ensm.2020.07.025.

Xiong, S., Chen, X., Liu, Y., Fan, T., Wang, Q., Zhang, H., and Chen, T. (2020). Black phosphorus as a versatile nanoplatform: From unique properties to biomedical applications. J. Innovative Opt. Health Sci. *13*, 2030008. https://doi.org/10.1142/S1793545820300086.

Yadav, T.P., Shirodkar, S.N., Lertcumfu, N., Radhakrishnan, S., Sayed, F.N., Malviya, K.D., Costin, G., Vajtai, R., Yakobson, B.I., Tiwary, C.S., and Ajayan, P.M. (2018). Chromiteen: a new 2D oxide magnetic material from natural ore. Adv. Mater. Inter. *5*, 1–9. https://doi.org/10.1002/admi.201800549.

Yan, P., Ji, L., Liu, X., Guan, Q., Guo, J., Shen, Y., Zhang, H., Wei, W., Cui, X., and Xu, Q. (2021). 2D amorphous-MoO3-x@Ti_3C_2-MXene non-van der Waals heterostructures as anode materials for lithium-ion batteries. Nano Energy *86*, 106139. https://doi.org/10.1016/j.nanoen.2021.106139.

Yang, C.S., Shang, D.S., Liu, N., Shi, G., Shen, X., Yu, R.C., Li, Y.Q., and Sun, Y. (2017a). A synaptic transistor based on quasi-2D molybdenum oxide. Adv. Mater. *29*, 1–10. https://doi.org/10.1002/adma.201700906.

Yang, Y., Pu, H., Lin, T., Li, L., Zhang, S., and Sun, G. (2017b). Growth of monolayer MoS_2 films in a quasi-closed crucible encapsulated substrates by chemical vapor deposition. Chem. Phys. Lett. *679*, 181–184. https://doi.org/10.1016/j.cplett.2017.05.015.

Yang, K., Zhang, T., Wei, B., Bai, Y., Jia, S., Cao, G., Jiang, R., Zhang, C., Gao, E., Chang, X., et al. (2020a). Ultrathin high-κ antimony oxide single crystals. Nat. Commun. *11*, 7–12. https://doi.org/10.1038/s41467-020-16364-9.

Yang, S., Zhang, P., Nia, A.S., and Feng, X. (2020b). Emerging 2D materials produced via electrochemistry. Adv. Mater. *32*, 1907857. https://doi.org/10.1002/adma.201907857.

Yang, W., Li, J., Zhang, X., Zhang, C., Jiang, X., and Liu, B. (2019). Hydrothermal approach to spinel-type 2D metal oxide nanosheets. Inorg. Chem. *58*, 549–556. https://doi.org/10.1021/acs.inorgchem.8b02742.

Yang, Y., Qiu, X., Shi, W., Hou, H., Zou, G., Huang, W., Wang, Z., Leng, S., Ran, Y., and Ji, X. (2021). Controllable fabrication of two-dimensional layered transition metal oxides through electrochemical exfoliation of non-van der Waals metals for rechargeable zinc-ion batteries. Chem. Eng. J. *408*, 127247. https://doi.org/10.1016/j.cej.2020.127247.

Yao, Q., Ren, G., Xu, K., Zhu, L., Khan, H., Mohiuddin, M., Khan, M.W., Zhang, B.Y., Jannat, A., Haque, F., et al. (2019). 2D plasmonic tungsten oxide enabled ultrasensitive fiber optics gas sensor. Adv. Opt. Mater. *7*, 1901383. https://doi.org/10.1002/adom.201901383.

Yin, P., Li, G., Zhang, B., Farjana, H., Zhao, L., Qin, H., Hu, B., Ou, J., and Tian, J. (2021). Facile PEG-based isolation and classification of cancer extracellular vesicles and particles with label-free surface-enhanced Raman scattering and pattern recognition algorithm. Analyst *146*, 1949–1955. https://doi.org/10.1039/d0an02257h.

Yu, J., Li, J., Zhang, W., and Chang, H. (2015). Synthesis of high quality two-dimensional materials via chemical vapor deposition. Chem. Sci. *6*, 6705–6716. https://doi.org/10.1039/c5sc01941a.

Yuan, T., Hu, Z., Zhao, Y., Fang, J., Lv, J., Zhang, Q., Zhuang, Z., Gu, L., and Hu, S. (2020). Two-dimensional amorphous SnO_x from liquid metal: mass production, phase transfer, and electrocatalytic CO_2 reduction toward formic acid. Nano Lett. *20*, 2916–2922. https://doi.org/10.1021/acs.nanolett.0c00844.

Zavabeti, A., Jannat, A., Zhong, L., Haidry, A.A., Yao, Z., and Ou, J.Z. (2020). Two-dimensional materials in large-areas: synthesis, properties and applications. Nanomicro Lett. *12*, 66. https://doi.org/10.1007/s40820-020-0402-x.

Zavabeti, A., Aukarasereenont, P., Tuohey, H., Syed, N., Jannat, A., Elbourne, A., Messalea, K.A., Zhang, B.Y., Murdoch, B.J., Partridge, J.G., et al. (2021). High-mobility p-type semiconducting two-dimensional β-TeO_2. Nat. Electron. *4*, 277–283. https://doi.org/10.1038/s41928-021-00561-5.

Zavabeti, A., Ou, J.Z., Carey, B.J., Syed, N., Orrell-Trigg, R., Mayes, E.L.H., Xu, C., Kavehei, O., O'Mullane, A.P., Kaner, R.B., et al. (2017). A liquid metal reaction environment for the room-temperature synthesis of atomically thin metal oxides. Science *358*, 332–335. https://doi.org/10.1126/science.aao4249.

Zavabeti, A., Zhang, B.Y., de Castro, I.A., Ou, J.Z., Carey, B.J., Mohiuddin, M., Datta, R.S., Xu, C., Mouritz, A.P., McConville, C.F., et al. (2018). Green synthesis of low-dimensional aluminum oxide hydroxide and oxide using liquid metal reaction media: ultrahigh flux membranes. Adv. Funct. Mater. *28*, 1–9. https://doi.org/10.1002/adfm.201804057.

Zhang, B.Y., Zavabeti, A., Chrimes, A.F., Haque, F., O'Dell, L.A., Khan, H., Syed, N., Datta, R., Wang, Y., Chesman, A.S.R., et al. (2018). Degenerately hydrogen doped molybdenum oxide nanodisks for ultrasensitive plasmonic biosensing. Adv. Funct. Mater. *28*, 1–13. https://doi.org/10.1002/adfm.201706006.

Zhang, C., John), J., Park, S.H., O'Brien, S.E., Seral-Ascaso, A., Liang, M., Hanlon, D., Krishnan, D., Crossley, A., McEvoy, N., et al. (2017). Liquid exfoliation of interlayer spacing-tunable 2D vanadium oxide nanosheets: high capacity and rate handling Li-ion battery cathodes. Nano Energy *39*, 151–161. https://doi.org/10.1016/j.nanoen.2017.06.044.

Zhuang, G., Yan, J., Wen, Y., Zhuang, Z., and Yu, Y. (2020). Two-dimensional transition metal oxides and chalcogenides for advanced photocatalysis: Progress, challenges, and opportunities. Sol. RRL. *2000403*, 1–50. https://doi.org/10.1002/solr.202000403.

Zhang, H. (2015). Ultrathin two-dimensional nanomaterials. ACS Nano *9*, 9451–9469. https://doi.org/10.1021/acsnano.5b05040.

Zhao, H., Zhu, Y., Li, F., Hao, R., Wang, S., and Guo, L. (2017). A generalized strategy for the synthesis of large-size ultrathin two-dimensional metal oxide nanosheets. Angew. Chem. Int. Ed. Engl. *56*, 8766–8770. https://doi.org/10.1002/anie.201703871.

Zhang, J., Lin, X., Xue, D., Xu, B., Long, D., Xue, F., Duan, X., Ye, W., Wang, M., and Li, Q. (2019). A generalized strategy for the synthesis of two-dimensional metal oxide nanosheets based on a thermoregulated phase transition. Nanoscale *11*, 3208–3215. https://doi.org/10.1039/c8nr09326a.

Zhang, B.Y., Xu, K., Yao, Q., Jannat, A., Ren, G., Field, M.R., Wen, X., Zhou, C., Zavabeti, A., and Ou, J.Z. (2021a). Hexagonal metal oxide monolayers derived from the metal–gas interface. Nat. Mater. *20*, 1073–1078. https://doi.org/10.1038/s41563-020-00899-9.

Zhang, L., Zhou, Y., Zheng, X., Jiang, J., and Xu, Q. (2021b). 2D nonlayered ferromagnetic VO_2 (M) nanosheets induced by the strain engineering of CO_2. Chem. Commun. *2*, 2–5. https://doi.org/10.1039/d1cc02269e.

Zeng, M., and Fu, L. (2018). Controllable fabrication of graphene and related two-dimensional materials on liquid metals via chemical vapor deposition. Acc. Chem. Res. *51*, 2839–2847. https://doi.org/10.1021/acs.accounts.8b00293.

Zhou, N., Yang, R., and Zhai, T. (2019). Two-dimensional non-layered materials. Mater. Today Nano. *8*, 100051. https://doi.org/10.1016/j.mtnano.2019.100051.

Zhang, T., and Fu, L. (2018). Controllable chemical vapor deposition growth of two-dimensional heterostructures. Chem *4*, 671–689. https://doi.org/10.1016/j.chempr.2017.12.006.

Zhang, W., Naidu, B.S., Ou, J.Z., Mullane, A.P.O., Carey, B.J., Wang, Y., Tang, S., Sivan, V., Mitchell, A., and Bhargava, S.K. (2015). Liquid metal/metal oxide frameworks with incorporated Ga_2O_3 for photocatalysis. ACS Appl. Mater. Inter. *7*, 1943–1948. https://doi.org/10.1021/am5077364.

Zhang, W., Ou, J.Z., Tang, S.Y., Sivan, V., Yao, D.D., Latham, K., Khoshmanesh, K., Mitchell, A., O'Mullane, A.P., and Kalantar-Zadeh, K. (2014).

Liquid metal/metal oxide frameworks. Adv. Funct. Mater. *24*, 3799–3807. https://doi.org/10.1002/adfm.201304064.

Zhao, S., Wang, L., and Fu, L. (2019). Precise vapor-phase synthesis of two-dimensional atomic single crystals. iScience *20*, 527–545. https://doi.org/10.1016/j.isci.2019.09.038.

Zhao, H., Li, F., Wang, S., and Guo, L. (2021a). Wet chemical synthesis of amorphous nanomaterials with well-defined morphologies. Acc. Mater. Res. *2*, 804–815. https://doi.org/10.1021/accountsmr.1c00104.

Zhao, S., Zhang, J., and Fu, L. (2021b). Liquid metals: a novel possibility of fabricating 2D metal oxides. Adv. Mater. *33*, 1–14. https://doi.org/10.1002/adma.202005544.

Zhou, S., Gan, L., Wang, D., Li, H., and Zhai, T. (2018). Space-confined vapor deposition synthesis of two dimensional materials. Nano Res. *11*, 2909–2931. https://doi.org/10.1007/s12274-017-1942-3.